Arkansas Bulletin of Water Research

A publication of the Arkansas Water Resources Center

Issue 2023

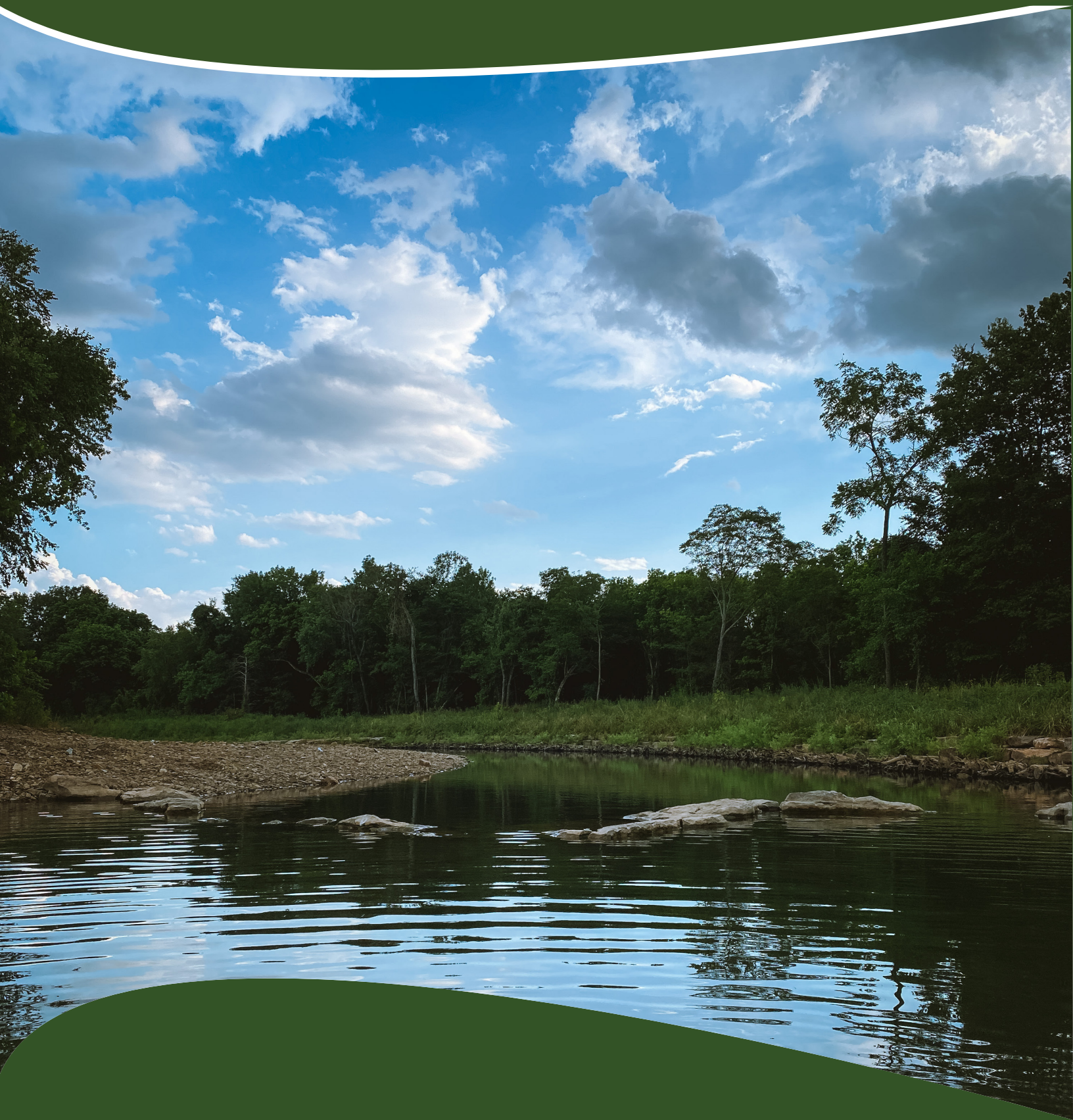

Arkansas Bulletin of Water Research

A publication of the Arkansas Water Resources Center

University of Arkansas
Don Tyson Center for Agricultural Sciences
1371 W. Altheimer Drive
Room 133
Fayetteville, AR 72704

website: awrc.uada.edu

EDITORS

Erin Grantz*
Arkansas Water Resources Center
Program Manager
egrantz@uark.edu
479-575-7192

Lillie Haddock
Arkansas Water Resources Center
Program Specialist
lmhaddoc@uada.edu

Brian E. Haggard
Arkansas Water Resources Center
Director
haggard@uark.edu
479-575-2879

**Corresponding author*

The Arkansas Bulletin of Water Research (Bulletin) is a publication of the Arkansas Water Resources Center (AWRC). We publish the Bulletin to communicate the major findings of research funded by the Water Resources Research Act Section 104(b) in Arkansas. This research is relevant to Arkansas water stakeholders, and the Bulletin provides an easily searchable and aesthetically engaging access option.

This is the fourth publication of the Bulletin. This issue contains final reports from research projects that were funded by the 104(b) program in fiscal years 2019 and 2020. The articles in this issue can be cited as an AWRC publication. Many of these projects have also appeared in peer-reviewed journal articles, which we recommend reviewing for greater detail or for updates on the findings presented here.

Please cite articles in the 2023 issue of the Bulletin, as in the following example:

Dodd, A., M. Bossus, and E. Pollock. 2023. Continuation: Nonpoint Source Pollution and Water Quality under Increasing Pressure from Poultry Agriculture in the Elevent Point and Lower Black River Watersheds. Arkansas Water Resources Center, Fayetteville, AR, Arkansas Bulletin of Water Research, 2023: 1-5.

The Bulletin is also available for outside submissions of research and investigations related to any water resources topic that is relevant for the State of Arkansas. This includes, but is not limited to, university researchers, consulting firms, watershed groups, and other agencies. Prospective authors should review the introductory material printed in earlier Bulletin issues and available at our website: **awrc.uada.edu**

The included material is based upon work supported by the U.S. Geological Survey 104(b) program under grant agreement No. G16AP00040 and G21AP10581 administered by the AWRC. The views and conclusions contained in this document are those of the authors and should not be interpreted as representing the opinions or policies of the U.S. Geological Survey.

Cover Photo: "West Fork of the White River" by Lillie Haddock

Arkansas Bulletin of Water Research

A publication of the Arkansas Water Resources Center

Issue 2023

Table of Contents

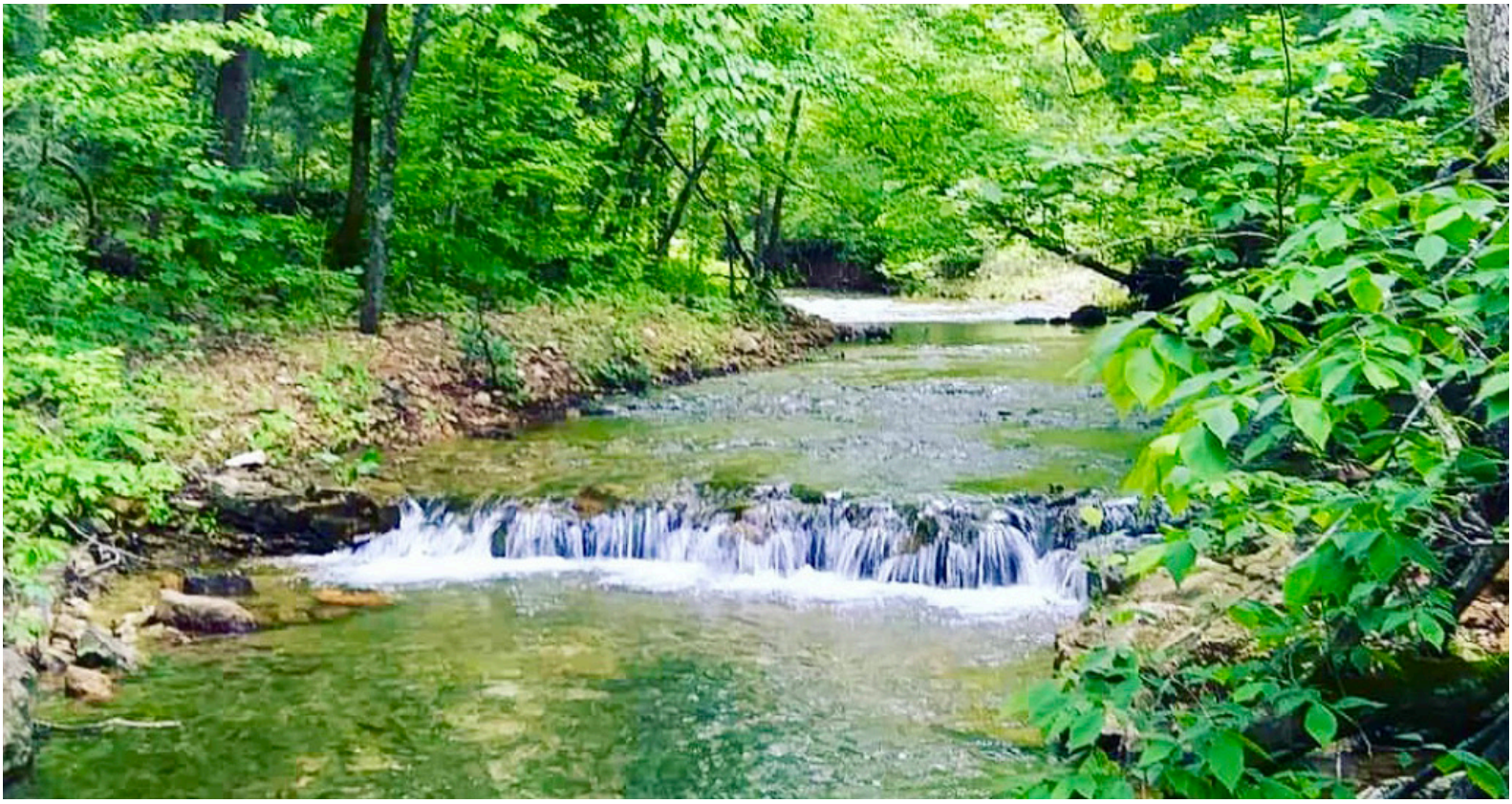

Image caption: Diles Creek, Photo Courtesy of Allyn Dodd

Continuation: Nonpoint Source Pollution and Water Quality under Increasing Pressure from Poultry Agriculture in the Eleven Point and Lower Black River Watersheds

Allyn Dodd[1], Maryline Bossus[2], and Erik Pollock[3]

[1]Biology Instructor, Arkansas School for Mathematics, Sciences, and the Arts, Hot Springs, AR 7190; [2]Assistant Professor of Biology, Lyon College, Batesville, AR 7250; [3]Director, Stable Isotope Laboratory, University of Arkansas, Fayetteville, AR 72701

Abstract: The expansion of poultry and livestock agriculture across Northeast Arkansas continues to threaten water quality and biological communities in critical waterways in the Mississippi Alluvial Plain. Following a 2019-2020 sampling campaign, we continued to sample twelve tributaries of the Eleven Point and Black rivers from April 2020 to February 2021 to determine if relationships existed between poultry and livestock agriculture and water quality, periphyton abundance, presence of algal toxins, and invertebrate community structure and physiology. Fewer pollution-intolerant macroinvertebrate species were found in streams close to poultry farm operations across both years of our study. We found no significant relationships between animal agriculture and stream nutrient levels. These results suggest that poultry farm operations near headwater streams pose a serious risk to the macroinvertebrate communities by reducing the abundance of sensitive taxa.

Key Points:

- Relative abundance of sensitive EPT taxa declined with increasing proximity to poultry houses.
- We found no relationship between nutrients or sediment concentrations and poultry or pastoral agriculture.
- We found no difference in expression in NKA in crayfish antennal or green glands across stream pollution levels.

Introduction

The installation of new poultry operations has exploded across Northeast Arkansas in the last four years. From 2017 to 2020, permits for 433 acres of new chicken houses have been issued (ADEQ, 2022). Each poultry house can hold 25,000 chickens, which translates to the potential of 20-30 million chickens at any given time regionally. As poultry houses are added to a landscape already affected by pastoral agriculture, the potential for nutrient and sediment loading to surface waters increases (McLauchlan, 2006). The potential for negative nutrient impacts to the watersheds and the need for data cannot be understated, especially given Arkansas's conflicted history of agriculture and water quality.

Rapid expansion of new poultry operations has been particularly heavy within the Eleven Point River watershed due to the construction of a new poultry processing facility in Pocahontas, Arkansas, in 2015. Prior to our previous efforts in 2019 and 2020, there was little monitoring of water quality and biological condition within the Eleven Point and Lower Black catchments, even as the potential for nonpoint source pollution rose throughout the area with the construction of more than 50 new chicken houses. This multi-year project specifically addresses the two nonpoint source pollution concerns the Arkansas Natural Resource Council (ANRC) has identified for Northeast Arkansas: nutrient and sediment loading from animal agriculture.

Results from prior sampling revealed that the percentage of EPT taxa observed was lower in tributaries found closer to poultry houses. However, no clear mechanism for declines in sensitive macroinvertebrates was detected during the first year of sampling, as we found no relationships between nutrients or sediment concentrations, or any instream variable, with poultry house density, flow path distance to poultry farms, or pastoral agriculture during the first year of study.

Our objective was to continue and expand the scope of our intensive monitoring program of water quality, harmful algal blooms, biological community structure, and organism pollution-related physiology throughout Eleven Point and Lower Black River catchments. We predicted that nutrient and total suspended solid concentrations would exhibit positive relationships with subwatershed poultry house density, subwatershed pastoral land use, and flow path distance to poultry farms. Algal biomass was also expected to increase with agricultural land use metrics. Sources of channel discharge throughout both drainages were expected to be dominated by groundwater. We hypothesized that macroinvertebrate communities in the upstream portions of the EPR drainage, which had fewer surrounding poultry farms, would contain greater amounts of intolerant taxa than habitats near the EPR outlet or throughout the LBR drainage. Additionally, physiological mechanisms such as osmoregulation of invertebrate bioindicators were predicted to be negatively impacted by pollution from nearby agricultural land. Indeed, elevated nitrogen in the environment stimulates growth of nitrifying bacteria which convert it to highly toxic ammonia. Ammonia is known to disrupt ionoregulatory function in crustaceans by increasing ion permeability (Spaargaren, 1990), and it is lethal at relatively low doses (Weihrauch et al., 2004). Crustaceans excrete excess ammonia mainly using their gills and antennal glands. The ammonia excretion rates are correlated with sodium absorption which is regulated by the activity of the pump Na^+/K^+-ATPase (NKA; Weihrauch et al., 2004). Therefore, we also assessed the impact of high nutrient concentrations in the environment on the expression and localization of NKA in a crustacean.

Methods

This study took place in 12 sites within the Eleven Point River and Lower Black River drainages along a gradient of animal agriculture and flow path distances from poultry houses. All sites have been identified from Year 1 of this project and are currently being sampled. Antecedent flow conditions will be determined by monitoring USGS gages throughout both watersheds. Water quality grab sampling, in situ measurements, and periphyton sampling took place during base flow conditions monthly from April 2020 through February 2021. We sampled two storm events over the sampling year in April and August of 2020. Duplicate water samples were collected at each site on each sampling date. Nitrate (NO_3^-) concentrations were determined using cadmium reduction. Filtered samples were subjected to the ascorbic acid method to determine soluble reactive phosphorus (SRP) concentrations. Total suspended solids were determined by vacuum filtration of samples and determining weight of previously suspended particles on pre-weighed filters (APHA, 2005). We collected samples for microcystin analysis in August of 2020.

Field parameters were collected using a handheld multiparameter probe (temperature, conductivity, pH). Habitat characteristics such as channel geometry and benthic substrate were also measured at each site. Periphyton from benthic rocks was collected throughout each reach for chlorophyll a to determine algal biomass. Invertebrates were collected at three riffles within each stream reach in June of 2020 and January of 2021 and identified to family (in the case of Chironomidae) and genus to determine invertebrate community structure and diversity.

Water quality and biological data were analyzed utilizing linear regression to identify whether relationships existed between instream variables and agricultural met-

rics (i.e. density of subwatershed poultry houses, pastoral land use, and flow path distance from poultry operations to study streams). We employed multiple linear regression analyses to pinpoint what instream variable(s) explain the greatest amount of variation in periphyton abundance and macroinvertebrate diversity across study sites. We compared stream and invertebrate metrics across years using t-tests to compare years one and two of the study.

Expression of NKA transcripts in Faxonius ozarkae sampled from a non-polluted creek (Diles) and two polluted creeks (Tennessee and Mill-Black) was analyzed in the antennal gland of 10 organisms per creek, using the method described in our previous report.

Results and Discussion

We found no significant relationships between average measures of physicochemical variables at base or storm flow and subwatershed poultry house density, pastoral land use, or flow path distance (Table 1). Preliminary data analysis in summer 2019 showed that, after removing an outlier (Hubble Creek) with low poultry house density but high P levels, there was a positive relationship between subwatershed poultry house density and stream phosphorus concentrations (R^2 = 0.84, p= 0.001), suggesting a seasonal component to poultry effects on stream water quality. However, we found no relationship between P and poultry agriculture in the second year of sampling (R^2 = 0.15, p = 0.63). Additionally, summer and annual storm samples did not exhibit significant relationships between nitrogen and phosphorus and surrounding poultry house density.

Soluble reactive phosphorus varied from 18 to 55 µg/L at base flow, with maximum P concentrations found in Upshaw Creek, which is situated near a poultry operation that frequently had chicken feathers in the stream. Measures of physicochemical variables from each stream at base flow can be found in Table 2. Table 3 shows nutrient and sediment concentrations from storm samples collected in June of 2019.

Algal biomass was not related to any instream variable (such as nutrient concentrations, total suspended solids, or discharge) (R^2 = 0.62, p = 0.22), nor poultry house density, pastoral land use, and flow path distance (R^2 = 0.40, p= 0.35) (Table 4). Chlorophyll a was below 5 mg/cm^2 across most sites (Table 5), though one site in the Eleven Point watershed, Mill-11, revealed elevated concentrations of chlorophyll a (15.0 mg/cm^2). No poultry operations were immediately upstream of the site and nutrient concentrations were not elevated, but the stream flowed through an area with very little canopy cover, likely driving greater rates of photosynthesis.

For the second year in a row, the proportion of Ephemeroptera, Plecoptera, and Trichoptera (EPT) taxa in sam-

Table 1: Results of multiple linear regression analyses between stream physicochemical variables and agricultural metrics (subwatershed poultry farm density, flow path distance from poultry operations to stream, and percent pastoral land use).

Dependent Variable	Independent Variables	R^2	p
Soluble Reactive Phosphorus	Poultry Density + Percent Pasture + Flow Path Distance (for all dependent variables)	0.02	0.97
Total Nitrogen		0.37	0.27
Nitrate		0.41	0.22
Total Organic Carbon		0.50	0.12
TSS		0.04	0.95
TSS		0.38	0.25

Table 2: Mean values of instream physicochemical variables and agricultural metrics at base flow. Mill-11 Pt. denote Mill Creek in the Eleven Point River watershed near Dalton, AR. Mill-Black denotes a different Mill Creek in the Lower Black watershed in Pocahontas, AR.

Site	Poultry House Density (km^2)	Percent Pasture	Flow Path Distance (m)	Discharge (cfs)	SRP (µg/L)	Total N (mg/L)	NO_3^- (mg/L)	TOC (mg/L)	TSS (mg/L)	Temperature (°C)	Conductivity (µS/cm)	Dissolved Oxygen (mg/L)	pH
Curia	0.26	30.10	3017	174.81	21.26	0.63	0.38	4.91	12.62	14.29	297	6.45	7.50
Cypress	0.21	26.90	1694	26.13	22.38	2.59	1.31	70.01	12.80	13.25	319	8.57	7.37
Diles	0.00	26.70	6201	7.77	33.97	0.78	0.32	52.38	14.20	15.27	160	8.86	6.13
Dota	0.57	42.90	1060	97.47	24.33	1.11	1.02	1.56	18.51	13.98	360	6.92	5.99
Eassis	0.17	30.10	871	38.14	18.43	1.91	0.95	68.74	9.12	13.23	285	9.21	8.03
Hubble	0.11	32.40	707	36.37	20.42	1.39	1.35	43.33	11.01	13.08	306	5.99	6.83
Knotts	0.06	30.20	1548	15.19	18.13	0.91	0.71	33.18	9.07	15.62	62	6.03	7.15
Lick	0.21	37.30	390	7.06	31.52	1.00	0.91	8.65	17.13	13.50	352	6.02	5.63
Mill-11 Pt.	0.00	42.30	996	170.92	22.68	1.23	1.16	48.99	15.57	13.52	286	10.86	7.16
Mill-Black	0.16	51.60	1915	27.90	21.15	1.23	1.21	50.31	27.64	13.31	346	7.90	5.84
Tennessee	0.06	35.20	163	86.87	25.83	2..60	1.29	66.38	21.82	14.74	319	8.53	6.65
Upshaw	0.10	28.20	531	17.30	54.83	1.45	1.42	70.10	10.56	13.67	404	6.31	6.29

ples was lower in streams closer to poultry operations ($p = 0.02$) (Figure 1). However, we still found no clear mechanism for declines in sensitive taxa near poultry operations. EPT taxa richness was greatest in Diles Creek (67%), just as it was in 2019. Diles Creek has the lowest subwatershed poultry house density and greatest distance to poultry operations. EPT richness was lowest in Upshaw Creek (4.71%) for the second consecutive year as well, which was in a subwatershed with low poultry house density but was directly adjacent to a poultry farm.

No relationships were observed between Shannon's diversity index, macroinvertebrate abundance, and any instream variable or surrounding animal agriculture (Shannon's: $R^2 = 0.29$, $p = 0.60$; Abundance: $R^2 = 0.07$, $p = 0.88$). Shannon's diversity varied from 0.78 to 2.09, with the lowest diversity as well as the lowest abundance of invertebrates found at Hubble Creek. Abundance was greatest at Tennessee Creek, had relatively low poultry house density within its subwatershed. Shannon's Diversity was greatest at Knott's Creek, which was also couched within a low poultry density subwatershed adjacent to Tennessee Creek.

We found no differences between any instream metrics across years with the exception of total organic carbon. We also found no differences in expression levels of NKA in the antennal gland in between organisms sampled from non-polluted and polluted creeks, similar to our results in gills and intestine previously reported.

Table 3: Mean values of soluble reactive phosphorus (SRP), nitrate (NO_3^-), and total suspended solids (TSS) from storm samples collected in April and August 2020.

Site	Storm SRP (µg/L)	Storm NO_3^- (mg/L)	Storm TSS (mg/L)
Curia	207.33	0.75	21.22
Cypress	183.49	1.61	11.70
Diles	54.88	0.92	22.27
Dota	230.47	1.72	40.38
Eassis	71.16	0.91	15.31
Hubble	249.42	2.08	20.50
Knotts	129.65	1.27	17.33
Lick	204.53	1.36	17.95
Mill-11 Pt.	100.58	1.92	22.27
Mill-Black	153.14	1.35	14.26
Tennessee	273.60	1.56	29.46
Upshaw	74.53	1.43	16.21

Conclusions

Two years of sampling have revealed that poultry agriculture negatively affects the proportion of sensitive macroinvertebrate taxa in tributaries of the Lower Black and Eleven Point Rivers. These findings benefit Arkansas water resource managers by pinpointing streams where pollution-intolerant macroinvertebrates are exhibiting susceptibility to land use change for new poultry operations. This research assists the USGS in addressing pressing water issues by providing evidence that proximity to poultry agriculture leads to sustained declines in sensitive macroinvertebrates.

Table 4: Results of multiple linear regression analyses between algal biomass, macroinvertebrate indices (Shannon's diversity, abundance, and percent EPT taxa), and their respective candidate models. Asterisks denote significant models. Italicized independent variables under a candidate model show individual p-values for each model parameter to illustrate primary drivers explaining variation in the dependent variable.

Dependent Variable	Independent Variables	R^2	p
Chlorophyll a	Poultry Density + Percent Pasture + Flow Path Distance	0.40	0.35
	SRP + NO_3^- + TSS + TOC + Discharge	0.62	0.22
Shannon's Diversity	Poultry Density + Percent Pasture + Flow Path Distance	0.29	0.60
	SRP + NO_3^- + TSS + TOC + Discharge	0.66	0.17
	Chlorophyll a	0.12	0.27
Abundance	Poultry Density + Percent Pasture + Flow Path Distance	0.07	0.88
	SRP + NO_3^- + TSS + TOC + Discharge	0.40	0.58
	Chlorophyll a	0.01	0.74
Percent EPT Taxa	Poultry Density + Percent Pasture + Flow Path Distance	0.56	0.08
	Poultry Density		0.47
	Percent Pasture		0.73
	Flow Path Distance		0.02*
	SRP + NO_3^- + TSS + TOC + Discharge	0.46	0.50
	Chlorophyll a	0.21	0.13

Table 5: Mean values of algal biomass, microcystin, and macroinvertebrate metrics.

Site	Microcystin (µg/L)	Chlorophyll a (µg/cm²)	Shannon's Diversity	Abundance	Percent EPT Taxa
Curia	0.203	3.39	2.05	111	47.75
Cypress	0.111	0.36	1.78	352	13.64
Diles	0.020	2.21	2.04	765	67.06
Dota	0.005	4.91	1.89	214	25.70
Eassis	0.006	4.09	1.60	738	33.88
Hubble	0.020	0.86	0.78	38	21.05
Knotts	0.002	0.54	2.09	93	11.83
Lick	0.009	0.32	1.24	295	1.69
Mill-11 Pt.	0.016	15.00	2.07	149	64.43
Mill-Black	0.005	1.58	1.84	426	31.46
Tennessee	0.121	2.86	1.16	1106	8.23
Upshaw	0.057	2.20	1.93	157	18.47

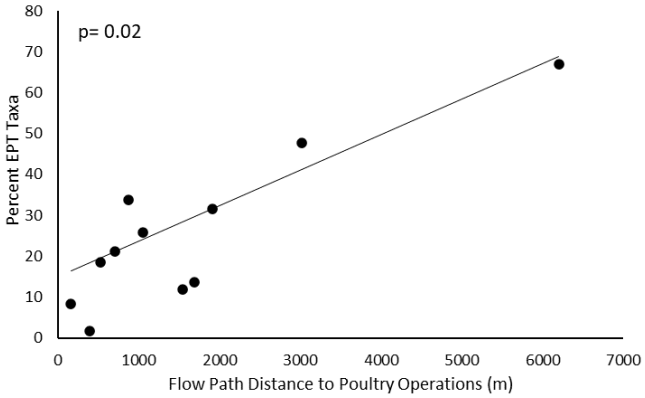

Figure 1: Percent EPT taxa versus flow path distance in meters from poultry operations.

Acknowledgements

This material is based upon work supported by the United States Geological Survey under grant agreement No. G16AP00040 and administered by the Arkansas Water Resources Center. The views and conclusions contained in this document are those of the authors and should not be interpreted as representing the opinions or policies of the U.S. Geological Survey.

References

American Public Health Association (APHA). 2005. Standard methods for the examination of water and wastewater, 21st ed., Washington, DC.

Arkansas Department of Environmental Quality. 2022. Final General Stormwater NPDES Permits Database. Accessed January 25, 2022.

McLauchlan, K. 2006. The nature and longevity of agricultural impacts on soil carbon and nutrients: A review. Ecosystems 9(8): 1364-1382.

Miller, S.M. and Wilkerson, T.F. 2000. Eleven Point River Watershed Inventory and Assessment. Missouri Department of Conservation, West Plains, Missouri.

Spaargaren, D.H. 1990. The effect of environmental ammonia concentrations on the ion-exchange of shore crabs, Carcinus maenas (L.). Comparative Biochemistry and Physiology part C 97, 87-91.

Weihrauch, D., Morris, S., Towle, D.W. 2004. Ammonia excretion in aquatic and terrestrial crabs. The Journal of Experimental Biology, 207, 4491-4504.

Image caption: Sam at work in the lab. Photo courtesy of Julian Fairey.

Moving Beyond Grab Sampling for Micropollutants in Water Systems: Diffusion Coefficient Measurements and Film Layer Thickness Assessments in Passive Sampler Hydrogels

Samuel D. Hodges[1] and Julian L. Fairey[2]

[1]PhD Candidate, Civil Engineering, University of Arkansas, Fayetteville, Arkansas 72701, [2]Associate Professor, Civil Engineering, University of Arkansas, Fayetteville, Arkansas 72701

Abstract: This report details an experimental protocol for a custom-fabricated two compartment diffusion cell (DC) and finite difference model (FDM) to determine micropollutant diffusion coefficients in the hydrogel layer (D_{Gel}) of a passive sampler. Passive sampling devices (PSDs) provide time-weighted-average concentrations of target analytes and, compared to grab sampling, more closely represent actual human exposures to micropollutants such as per- and polyfluoroalkyl substances (PFAS) and disinfection byproducts (DBPs). Nitrate was selected as a surrogate micropollutant and was assessed in a series of DC tests as a function of hydrogel thickness (δ_{Gel}) to determine D_{Gel} for nitrate through two gel types and the diffusion boundary layer thickness (δ_{DBL}) at six DC mixing speeds. The principal findings were 1) A compartment mixing speed of 500 RPM was sufficient to make δDBL negligible relative to δ_{Gel} and is recommended for D_{Gel} measurements of micropollutants such as PFAS and DBPs. 2) The FDM does not rely on simplifying assumptions made in traditional D_{Gel} analyses and allows for assessment of D_{Gel} at concentration ranges relevant in water systems. The protocol developed here can be applied to measure D_{Gel} for PFAS and DBPs. These values can then be used to inform the design of diffusive gradients in thin-films (DGT) PSDs for deployments in natural waters and drinking water systems as an alternative to traditional grab sampling.

Key Points:

- Passive samplers provide time-weighted concentrations of micropollutants in water systems and improved chronic exposure assessments relative to grab sampling
- Fabricated a two-compartment diffusion cell was to measure analyte diffusion coefficients in hydrogels to support development of diffusive gradients in thin-films passive samplers
- Formulated a finite difference model to determine diffusion coefficients and assess diffusive boundary layer thicknesses as a function of mixing speed
- Determined a mixing speed of 500 RPM was sufficient to minimize the diffusive boundary layer thickness and is recommended for measurements of analyte diffusion coefficients

Introduction

In 2022, the Environmental Protection Agency (EPA) published two notices regarding per- and polyfluoroalkyl substances (PFAS) in drinking water which include (1) the Unregulated Contaminant Monitoring Rule 5 (UCMR5) which requires drinking water utilities to sample for 29 PFAS and lithium starting in January 2023 and (2) a health advisory which lists four PFAS and concentration thresholds over which chronic exposures may cause harm to human health. These regulatory notices require PFAS measurements by grab sampling, a technique which may differ from the time-weighted average concentrations to which consumers are exposed to chronic pollutants such as PFAS and disinfection byproducts (DBPs). Over the past three decades, the diffusive gradients in thin-films (DGT) passive sampling device (PSD) has been investigated extensively and used to determine time-weighted-average (TWA) concentrations of micropollutants in rivers, lakes, wells, oceans, wastewater effluents, and other waters.

DGT consists of a dowel-plunger assembly with an outer membrane filter covering a diffusive gel layer backed with a binding layer (see Figure 1).

Analytes present in the bulk water sorb in the binding layer of a DGT-PSD at a rate proportional to their mass transport through the diffusive gel layer. In principal, a DGT-based measurement is well-suited for contaminants such as PFAS and DBPs from which harm to human health is based on chronic exposures. DGT deployment times can be tuned by adjusting the thickness of the diffusive gel layer, which ranges from 0.080–0.20 cm, and typically ranges from a few days to a couple months. Analyte mass will accumulate in the DGT-PSD binding layer at any bulk water concentration, including at pg•L^{-1} levels, albeit longer deployment times may be needed to detect these levels. Thus, DGT-PSDs are a potential alternative to grab sampling for monitoring PFAS and DBP levels in drinking water systems.

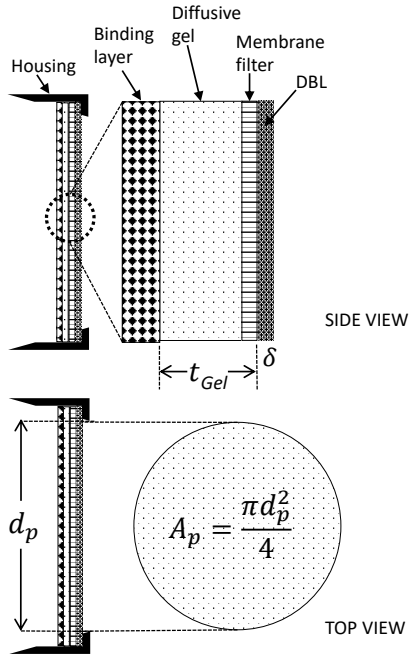

Figure 1: Top and side views of the layers in a diffusive gradients in thin-films (DGT) passive sampling device (PSD)

To determine bulk water concentrations from a DGT-PSD, diffusion coefficients in the hydrogel, D_{Gel}, must be known. The most common method for determining DGel involves using a two-compartment diffusion cell (DC) (Guibal et al., 2019), which consists of well-mixed source and sink compartments bridged together by the diffusive gel of known thickness, δ_{Gel}, and area. Equation 1 shows Fick's first law which describes one-dimensional diffusive flux from a region of higher to lower concentration, where J is the diffusional flux, C is concentration, and x is the position relating to diffusive length:

$$J = -D\,\partial C/\partial x \qquad \text{Equation 1}$$

Figure 2 shows a schematic view of the gel bridge in a two-compartment DC. At time zero, the source compartment is dosed with the target analyte(s) to provide a driving force for diffusion across the hydrogel. Temporal samples are taken from the source and sink over the course of a few hours to a few days to determine their respective concentrations, C_{Source} and C_{Sink}.

In traditional DC analyses, the following assumptions are made based on the work of others (Zhang & Davison, 1999) and Equation 2 is used to calculate D_{Gel} using, α, the slope of the sink mass vs. time profile, δ_{Gel}, the hydrogel thickness, A_p, the porthole area between the source and sink compartments, and $C_{Source\text{-}Avg}$, the average source concentration:

$$D_{Gel} = (\alpha \cdot \delta_{Gel})/(A_p \cdot C_{Source\text{-}Avg}) \qquad \text{Equation 2}$$

1. Compartment mixing is sufficiently fast such that the diffusion boundary layer (DBL) thickness, δ_{DBL}, is negligible relative to δ_{Gel} (i.e., $\delta_{Gel} >> \delta_{DBL}$)
2. The experimental duration is short (typically < 2 hours), such that C_{Source} is effectively constant (< 5% decrease)
3. C_{Sink} remains small such that $C_{Source} >> C_{Sink}$

Despite the ubiquity of two-compartment DC measurements in DGT literature, there are no detailed designs available for DC fabrication and no experimental evidence to assess if assumptions 1 and 3 are valid. Without a robust method to determine D_{Gel} values, it is not possible to

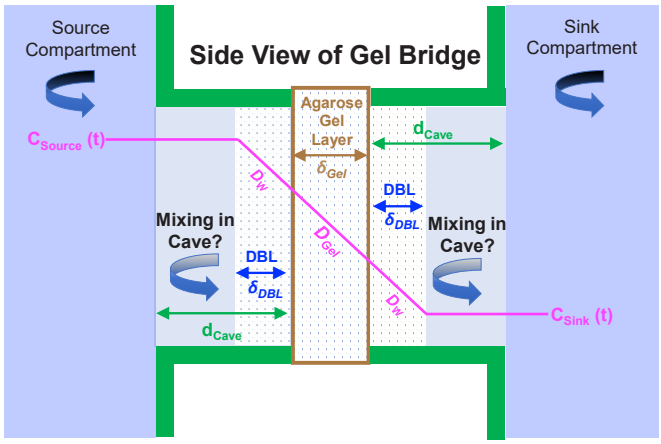

Figure 2: A conceptual scheme of the gel bridge in a two compartment diffusion cell (DC)

accurately assess micropollutants using DGT-PSDs. To resolve this issue, a custom fabricated two-compartment DC was used to assess D_{Gel} for nitrate as a function of gel type and gel thickness. A companion finite difference model (FDM) was formulated to determine D_{Gel} without the assumptions needed to apply Equation 2. This work facilitates determination of D_{Gel} for PFAS and DBPs and provides a fundamental foundation to apply DGT-PSDs for use in drinking water systems.

Methods

Chemicals and Reagents

All water used for reagent preparation had a resistivity of 18.2 MΩ•cm and was produced by a Thermo Fisher Scientific Smart2Pure 6 UV system. Trizma® pH 7 preset crystals (Sigma-Aldrich) were used for the DC experiments at pH 7, added at 500 mg•L-1 to limit the pH drift to ± 0.1 pH units and achieve conductivity of about 400 µS•cm^{-1}, similar to previous DC experiments with NO_3^- in freshwater systems (Huang et al., 2016). ACS grade potassium nitrate (KNO_3) was used without any further purification and a 0.1 M sodium chloride (NaCl) solution provided by DGT® Research (United Kingdom) was used for hydrogel storage.

Hydrogels

Two hydrogel types were acquired from DGT® Research and assessed in the DC experiments, which included (1) agarose crosslinked polyacrylamide (APA) standard diffusive gel discs, product number R-GDD, and (2) agarose diffusive gel discs (hereinafter agarose), product number R-GDA. Each gel type was acquired in four thicknesses, δ_{Gel}, of 0.080-, 0.12-, 0.16-, and 0.20 cm. Gels were refrigerated at 4°C and stored in ultrapure water and 0.1 M NaCl solution for the agarose and APA gels, respectively, as recommended by DGT® Research.

Nitrate Quantification in the DC Experiments

NO_3^- was quantified in the DC experiments using UVA at 203 nm (UV_{203}) similar to others (Huiru et al., 1991), measured in a 1.0 cm pathlength quartz cuvette with a UV/Vis spectrophotometer (Shimadzu 2450). The scan speed was 430 nm•min^{-1} and instrument reading stability (i.e., signal noise) was ± 0.001 absorbance units (A.U.). UVA spectra were collected from 400 nm down to 190 nm in 1 nm increments. Preliminary testing indicated that UV_{203} was impacted by pH, and as such, the pH drift was maintained within ± 0.2 pH units throughout each DC test using pH 5, 7, and 9 buffers, as detailed previously. The sample pH was measured at the start of each test using a Thermo Orion pH electrode calibrated using pH standards at 4, 7, and 10.

The pH 7 Trizma® buffer UV_{203} signal varied by batch from 0.031–0.11 A.U. over the 12-month sampling period. To account for the variability in the buffer signal, a minimum of three blank buffer samples were measured over the course of each experiment and the median signal was subtracted from the sample responses. Calibration curves with a minimum of five NO_3^- standards were collected and UV_{203} ranged from 0.005–1.8 A.U. NO_3^- standard curves between 0–2.8 mg•L^{-1}-N had $R^2 > 0.99$. To determine the NO_3^- concentration profiles in source and sink compartments, 1.5 mL sample volumes were collected from each compartment every 10 minutes for 3–72 hours as detailed in the next subsection. Source compartment samples were diluted 32:1 prior to measurement such that their UV_{203} signal was within the standard curve. UV_{203} of the sink compartment samples were measured without dilution.

Diffusion Cell Experiments

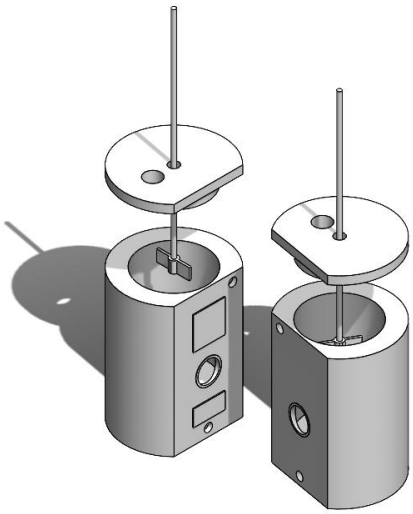

Figure 3: A SolidWorks rendering of the custom fabricated two compartment diffusion cell (DC) used for measurement of analyte diffusion coefficients in passive sampler hydrogel layers

A two-compartment DC was designed and fabricated from ultra-high molecular weight polyethylene for use with hydrogels acquired from DGT Research (Figure 3).

A principal design element of the DC was to minimize the depth of the so-called cave shown in Figure 2, in which incomplete fluid mixing may occur and thus lead to formation of a thicker DBL on either side of the hydrogel than would be expected based on the compartment mixing speed. The circular porthole connecting the Source and Sink compartments had a diameter of 1.70 cm which corresponded to a diffusive area A_p of 2.27 cm^2. Layers of 0.02 cm thick tape were used as variable thickness spacers that accommodated hydrogel thicknesses ranging from 0.080–0.20 cm. Following hydrogel installation in the DC but prior to each test, the source and sink compartments were simultaneously filled to 100 mL with buffered water. Each compartment was capped with a lid and mixed using a Caframo® BDC250 stirrer at rates of 100-, 200-, or 500 RPM for the duration of the experiment. At time zero, t_0, the source compartment was dosed with nitrate at a concentration which varied from 10–15 mg•L^{-1}-N. About 15–20 temporal samples were collected via sampling ports in the compartment lids using a 1 mL mechanical pipette (Eppendorf) and measured within a few minutes by UV spectroscopy. Upon completion of each experiment, the remaining water was emptied, and the DC disassembled, cleaned, and allowed to air dry. Forty-eight DC experiments were completed using the agarose gel type which included (1) triplicate experiments at all four hydrogel thicknesses at mixing speeds of 100-, 200-, and 500 RPM and (2) single experiments at all four hydrogel thicknesses at mixing speeds of 50-, 300-, and 400 RPM. Twenty-four DC experiments were completed using the APA gel type which included triplicate experiments at all four hydrogel thicknesses at mixing speeds of 200-, and 500 RPM.

Finite Difference Model

To determine the NO_3^- diffusion coefficient in the hydrogel, DGel, without the simplifying assumptions detailed in the introduction, a finite difference model (FDM) was developed in the freeware program R (Crawley, 2007) to analyze the DC kinetics. Here, analyte mass transport across a hydrogel of thickness δ_{Gel} was modeled as a 1-dimensional diffusion problem (Figure 4). Despite mixing in the Source and Sink compartment and minimization of d_{Cave} (Figure 2), a DBL of thickness δ_{DBL} will exist at both ends of the hydrogel layer where convective mass transport is negligible.

The analyte flux, J, through the DBL can be computed using Fick's first law (Equation 1). If the analyte concentration changes in the Source and Sink compartments are slow relative to the dynamics in the DBLs, analyte mass transport across the DBLs can be approximated using linear gradients where D_W is the analyte diffusion coefficient in water, which should be greater than D_{Gel}, and C is the aqueous phase analyte concentration at the hydrogel surface in the Source or Sink compartment. A finite difference model was determined and was used to construct an initial value problem that was solved using the deSolve package for R (Soetaert et al., 2010).

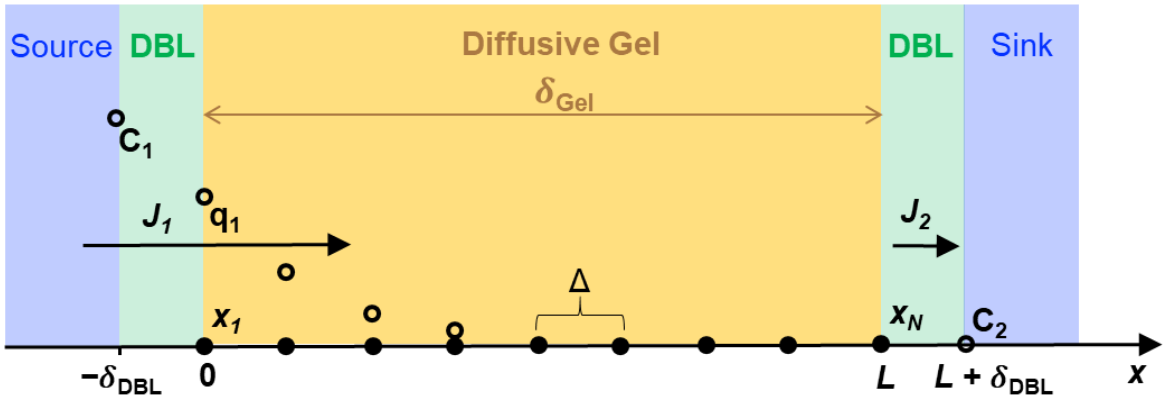

Figure 4: One-dimensional diffusion scheme depicting the diffusive gel layer and surrounding region in the two-compartment diffusion cell tests. Analyte(s) spiked into the source compartment at concentration C_1 diffuse into the sink compartment through a (i) source-side liquid film diffusive boundary layer (DBL) of thickness δ_{DBL} at flux J_1, (ii) diffusive gel layer of thickness δ_{Gel} at a gel surface concentration q_i with i = [1,…n], where n = 50, the number of equally-spaced grid points separated by a distance Δ in the x-direction and equal to L at n = 50, and (iii) a sink-side DBL of thickness δ_{DBL} assuming the mixing conditions in the source and sink are identical.

Table 1: Summary of the number of two-compartment diffusion cell (DC) tests completed to assess the diffusive boundary layer thickness (δ_{DBL}) as a function of compartment mixing speed for agarose and agarose crosslinked polyacrylamide (APA) gel types.

Group	Gel type	[a] Mixing Speed (RPM)	Gel Thickness, δ_{Gel} (cm)			
			0.080	0.12	0.16	0.20
A	Agarose	50	1	1	1	1
B	Agarose	100	3	3 (1)[b]	3	3
C	Agarose	200	3	3	3	3
D	Agarose	300	1	1	1	1 (0)[b]
E	Agarose	400	1 (0)[b]	1	1	1
F	Agarose	500	3	3	3	3
G	APA	200	3	3	3	3
H	APA	500	3	3	3	3

a Source and sink compartment were mixed at the specified speed for the duration of the tests
b Number of experiments used in the finite-difference model global fit after removing outlier(s) shown in parentheses

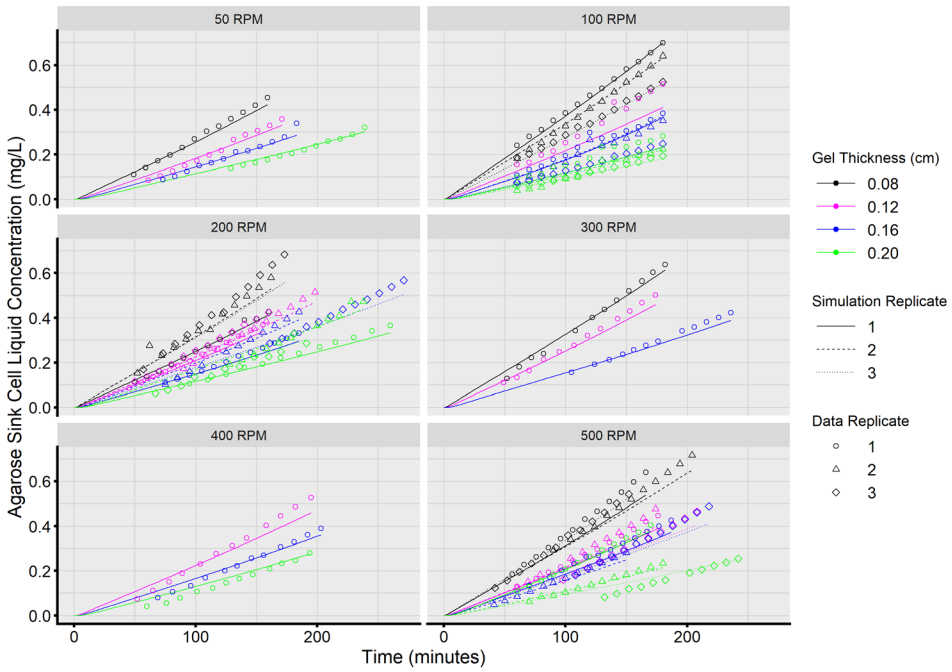

Figure 5: Sink compartment nitrate profiles for the two-compartment diffusion cell (DC) tests with agarose gel. Each panel shows measured concentrations (points) for a single mixing speed (see panel titles) in the source and sink compartments as a function of gel thickness (δ_{Gel}). The finite-difference model global fit (lines, see text) were generated with the best-fit D_{Gel} and δ_{Gel} shown in Table 2.

Results and Discussion

Table 1 lists the number of nitrate DC experiments used to assess δ_{DBL} as a function of compartment mixing speed. Figure 5 shows the sink compartment nitrate concentration profiles for 44 tests with the agarose gel type and Figure 6 shows the companion source concentration profiles.

Figure 5 shows for a given mixing speed and sample time, greater sink mass concentrations were measured with decreasing δ_{DBL}, an expected result that indicates nitrate diffusion to the sink varied indirectly with gel thickness. Figure 6 shows the source concentrations decreased less than 5% throughout a given test and the initial concentrations ranged from 10–23 mg•L^{-1}-N amongst the 44 tests. Figure 5 shows the sink concentrations increased throughout each test and were between about 0.05- and 0.7 mg•L^{-1}-N. The upper limit of this range was within two orders of magnitude of the source concentration, violating the simplifying assumption in typical DGT analyses that $C_{source} >> C_{sink}$ such as to produce unrestricted diffusion from the source to the sink compartments. Importantly, the FDM developed in this work does not rely on such a simplifying assumption and thus the concentrations ranges shown in Figures 5 and 6 were suitable for determining D_{Gel} and δ_{DBL}.

The FDM was used to simulate nitrate diffusion kinetics and determine (1) D_{Gel} for nitrate in agarose and APA gel types and (2) δ_{DBL} as a function of compartment mixing speed (50-, 100-, 200-, 300-, 400-, 500 RPM). Initial guesses of D_{Gel} were 13.8×10^{-6} cm•s^{-2} and δ_{DBL} ranged from 0.050–150 µm, depending on the mixing speed of the corresponding experimental group, A–H. The D_{Gel} estimate was based on D_{Gel} determinations for nitrate (Huang et al., 2016), adjusted for temperature using the Stokes-Einstein

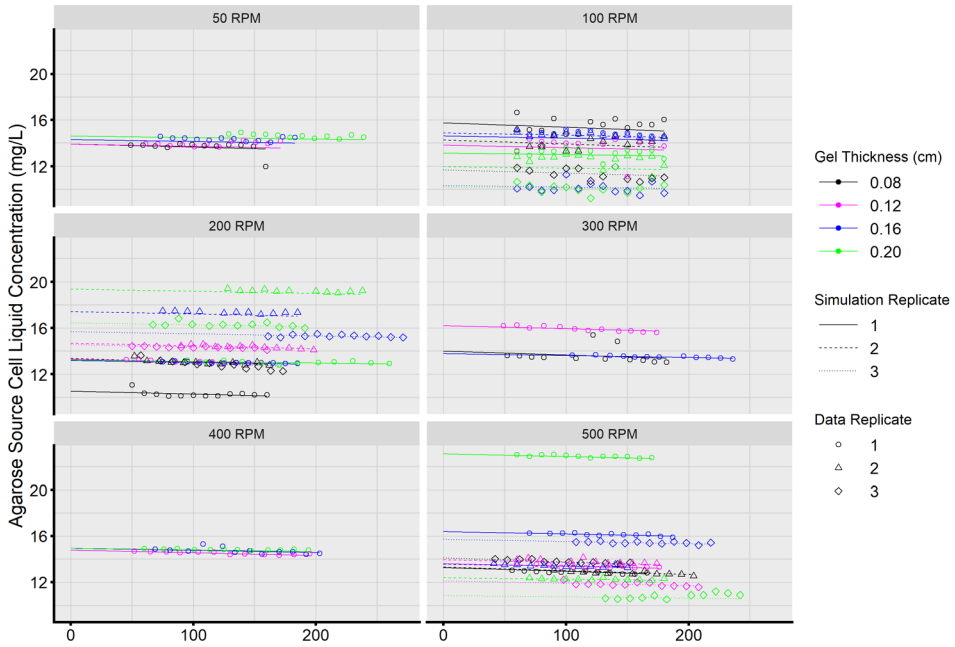

Figure 6: Source compartment nitrate profiles for the two-compartment diffusion cell (DC) tests with agarose gel. Each panel shows measured concentrations (points) for a single mixing speed (see panel titles) in the source and sink compartments as a function of gel thickness (δ_{Gel}). The finite-difference model (FDM) global fit (lines, see text) were generated with best-fit DGel and δ_{Gel} shown in Table 2.

Table 2: Summary of the FDM fitting parameters δ_{DBL} and D_{Gel} for the individual group fits and global fit of groups A–H for the two-compartment diffusion cell (DC) experiments.

	Group Fit to Minimize [a]WSSE			Global Fit of Groups A–H to Minimize [a]WSSE		
Group	δ_{DBL} (μm)	D_{Gel} (cm•s^{-2})	[a]WSSE	δ_{DBL} (μm)	D_{Gel} (cm•s^{-2})	[a]WSSE
A	100	13.0×10^{-6}	0.307	149	14.2×10^{-6}	13.0
B	7.5	14.5×10^{-6}	2.80	7.0		
C	1.0	14.3×10^{-6}	1.67	1.0		
D	7.5	12.0×10^{-6}	4.18	7.0		
E	25	12.0×10^{-6}	2.37	23.5		
F	1.0	14.8×10^{-6}	0.789	0.89		
G	50	14.0×10^{-6}	2.28	1.0	13.6×10^{-6}	2.28
H	1.0	14.0×10^{-6}	1.72	0.89		

[a] Weighted residual sum of square errors

equation.

Table 2 shows the D_{Gel} and δ_{DBL} combinations that minimized the weighted sum of squares error (WSSE) for each group and a global fit for all groups, A–H. Figure 7 shows a WSSE contour plot generated from arrays of D_{Gel} and δ_{DBL} combinations for the agarose gel type at 100 RPM. The best-fit D_{Gel} and δ_{DBL} combination that minimized the WSSE is indicated on the plot and listed for each group are listed in Table 2.

The best-fit D_{Gel} values for each group indicated D_{Gel} for the agarose gel type ranged from 12.0–14.8×10−6 cm^2•s^{-1}. However, D_{Gel} should be independent of mixing speed and thus be a constant value among Groups A–F. The FDM was therefore refit by gel type to determine a global fit for D_{Gel}. Initial guesses were taken to be the DBL values from the individual group fits (Table 2) and the average D_{Gel} values for agarose and APA gel types, which were 13.4×10^{-6} and 14.0×10^{-6} cm•s^{-2}, respectively. Following removal of four outlier experiments based on outsized contributions to the WSSE, the final dataset for the global fit consisted of 68 experiments. Nitrate D_{Gel} for the agarose and APA gel types were determined to be 14.2×10^{-6} and 13.6×10^{-6} cm•s^{-2}, respectively, the global WSSE was 13, and the values of δ_{DBL} are listed in Table 2 by group.

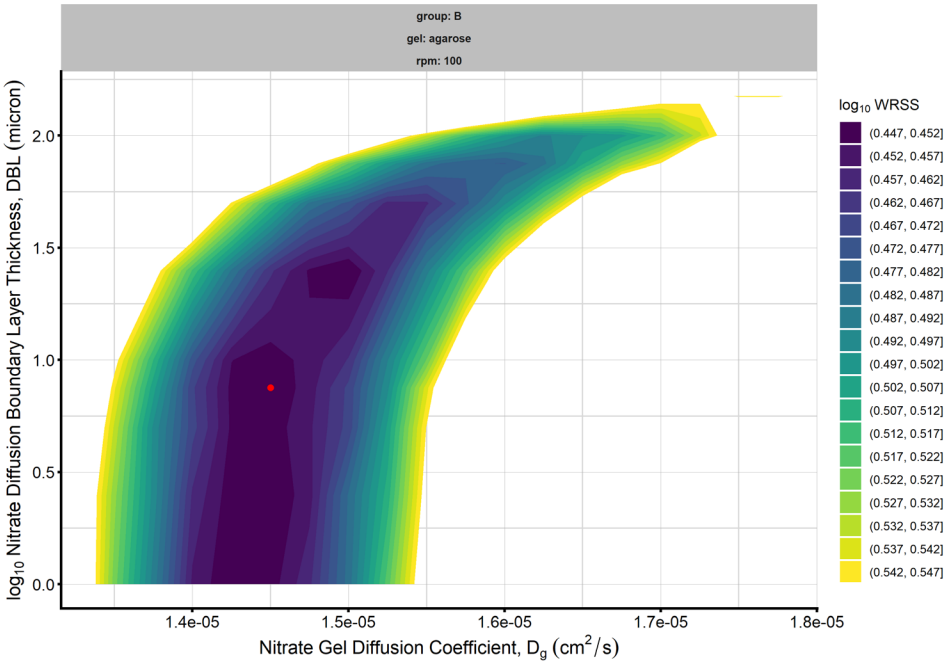

Figure 7: Contour plot of the weighted sum of square error (WSSE) of D_{Gel} and δ_{DBL} combinations in the finite difference model (FDM) for the Group B experiments completed at 100 RPM using the agarose gel type. The minimum WSSE is indicated by the red point at $D_{Gel} = 14.5 \times 10^{-6}$ cm$^2 \bullet$s^{-1} and $\delta_{DBL} = 7.5$ µm.

δ_{DBL} was expected to decrease with increasing mixing speed. The global results in Table 2 indicate that δ_{DBL} was 149 µm on either side of the gel at 50 RPM and < 1 µm at 500 RPM. However, there was no apparent trend in δ_{DBL} between 100–500 RPM, with δ_{DBL} ranging between 1–23.5 µm. Importantly, however, δ_{DBL} was insignificant at 500 RPM and thus is recommended for measuring D_{Gel} of other analytes in two-compartment diffusion cell tests.

Conclusions

A two compartment DC was designed and validated for use with micropollutants in water systems. A FDM was developed to eliminate the need for simplifying assumptions required for diffusion coefficient (D_{Gel}) determinations and assessments of diffusive boundary layer thickness (δ_{DBL}). These results could be leveraged to develop passive samplers based on the diffusive gradients in thin-films (DGT) technique to replace grab sampling for per- and polyfluoroalkyl substances (PFAS) and disinfection byproducts (DBPs) in drinking water systems.

Acknowledgements

This material is based upon work supported by the United States Geological Survey under grant agreement No. G21AP10581 and administered by the Arkansas Water Resources Center. The views and conclusions contained in this document are those of the authors and should not be interpreted as representing the opinions or policies of the U.S. Geological Survey.

References

Crawley, M. J. (2007). The R Book.

Guibal, R., Buzier, R., Lissalde, S., & Guibaud, G. (2019). Adaptation of diffusive gradients in thin films technique to sample organic pollutants in the environment: An overview of o-DGT passive samplers. Science of the Total Environment, 693. https://doi.org/10.1016/j.scitotenv.2019.07.343

Huang, J., Bennett, W. W., Teasdale, P. R., Gardiner, S., & Welsh, D. T. (2016). Development and evaluation of the diffusive gradients in thin films technique for measuring nitrate in freshwaters. Analytica Chimica Acta, 923, 74-81 , publisher = Elsevier Ltd. https://doi.org/10.1016/j.aca.2016.04.006

Huiru, D., Meiyu, J., & Qing, Z. (1991). Simultaneous Ultraviolet Spectrophotometric Determination of Nitrate and Nitrite in Water. Analytical Letters, 24(2), 305-315. https://doi.org/Doi 10.1080/00032719108052906

Soetaert, K., Petzoldt, T., & Setzer, R. W. (2010). Solving Differential Equations in R. Journal of Statistical Software, 2, 5-15. https://doi.org/10.32614/rj-2010-013

Zhang, H., & Davison, W. (1999). Diffusional characteristics of hydrogels used in DGT and DET techniques. Analytica Chimica Acta, 398, 329-340. https://doi.org/10.1016/S0003-2670(99)00458-4

Image caption: Drs. Jenny Richter and Phillip Owens describe a soil profile of a karst soil column, which will later be used to quantify nutrient macro pore flow and leaching. Photo courtesy of Amanda Ashworth.

Quantifying Bypass Flow in Terra Rosa Soils: Implications for Groundwater and Stream Contamination

Sheela Katuwal[1], Amanda J. Ashworth[2], Philip Owens[3], and Kristofor R. Brye[4]

[1]Post-doctoral fellow, Department of Poultry Science, University of Arkansas, Fayetteville, AR, 72701, [2]Soil scientist, USDA-ARS- Poultry Production and Product Safety Research Unit, Fayetteville, AR, 72701, [3]Research leader, USDA-ARS- Dale Bumpers Small Farms Research Center, Booneville, AR, 72927, [4]University Professor, Department of Crop, Soil, and Environmental Sciences, University of Arkansas, Fayetteville, AR, 72701

Abstract: Subsurface transport of phosphorus (P) in manure-amended soils through preferential flow pathways such as soil macropores can be a substantial non-point source of P pollution, although studies quantifying preferential flow P losses are lacking. We evaluated the role of preferential flow in P leaching losses from surface-applied poultry litter (5.6 Mg ha^{-1}) in intact soil columns (40 diameter × 100 cm height) collected from a karst and non-karst landscape (three replicates per soil) in Arkansas from three simulated rain events (3.9 cm h^{-1} for 2 hours). The extent of preferential flow in karst derived soil was greater than non-karst derived soil due to greater content of coarse fragments in soil. Dissolved P constituted more than 80% of the total P loss, which peaked (5.61 mg L^{-1}) following the first irrigation event after litter application and decreased to about half (2.88 mg L^{-1}) by the third irrigation event. Soils from karst landscapes greater ($p < 0.05$) volume of water and total P, with approximately six times greater losses than non-karst soils. We found that the top 1 m of soil from the karst landscape is vulnerable to vertical P transport into deeper soil layers and therefore, may have the potential to increase legacy P in subsurface soil and pose a threat to surface and groundwater over time.

Key Points:

- P loss in leachate was largely controlled by leachate volume and the extent of preferential flow pathways.
- Incidental increase in P loss occurred following P application.
- Karst soils leached six times greater P than non-karst soils and thus the overlying karst soils may increase legacy P and threaten water quality.

Introduction

Subsurface transport of phosphorus (P) from land-applied animal manures can be an important pathway for P losses to water bodies (King et al., 2015; Sims et al., 1998), yet only a limited number of P risk assessment models developed for regulating P additions in soils account for subsurface P losses (Radcliffe et al., 2015; Reid et al., 2012). Subsurface transport of P occurs via matrix flow and preferential flow. Preferential flow pathways (PFPs) such as soil macropores are markedly wider than matric flow passages, allowing water to move at a relatively high velocity (Jarvis, 2007). This limits the interaction between solutes in the flowing water and the soil, thereby resulting in rapid flow of solutes through PFPs (Mahmood-Ul-Hassan et al., 2010). Identification of PFPs specific to an area may be useful in developing tools for risk assessment of subsurface P transport from agricultural land to water bodies (Allaire et al., 2011).

Certain areas such as karst landscapes are particularly susceptible to subsurface losses owing to their vulnerability to have direct connectivity between soil surface and groundwater. Soils in karst landscapes may contain loose soil between coarse fragments, in addition to earthworm burrows, plant roots, and fissures, that channel flow through the soil (Sauer and Logsdon, 2002). In addition to these features common to karst landscapes, the mantled karst terrain of the Ozark Plateau in northwest (NW) Arkansas contains many confined animal-feeding operations where the resulting animal manure, particularly poultry litter (PL), is used to fertilize pastures (Sharpley et al., 2020). This adds to the vulnerability of the Ozarks region to increasing risks of surface and subsurface P losses from surface-applied PL to water bodies. The objectives of this study were to quantify and contrast P leaching losses through preferential transport from recently applied PL in large intact soil columns (40 cm diameter × 100 cm deep) obtained from the mantled karst terrain in NW Arkansas and a non-karst terrain in Arkansas. This quantification is needed for improving understanding of P transport with infiltrating water in soils of karst and non-karst landscapes and can aid in the implementation of customized manure management practices for minimizing P leaching losses in soils overlying karst systems.

Methods

Soils from pastures located in a mantled karst landscape in NW Arkansas near Savoy (36° 7' 28.2" N, 94° 18' 43.2" W) and in a non-karst landscape in Booneville, Arkansas (35° 5' 54.6" N, 93° 58' 10.2" W) were studied. Dominant soil series in the karst area are Clarksville (loamy-skeletal, siliceous, semiactive, mesic Typic Paleudults) and Nixa (loamy-skeletal, siliceous, active, mesic Glossic Fragiudults). The karst area received PL annually at the rate of 8.6 Mg ha^{-1} for about 15 years. The prominent soil series in Booneville is Leadvale (fine-silty, siliceous, semiactive, thermic Typic Fragiudults). Mean annual precipitation for NW Arkansas and Booneville are 1156 mm and 1265 mm, and the mean annual air temperatures are 14.5°C and 15.6°C, respectively (NOAA, 2021).

Intact soil columns (three per site), 40 cm in diameter and 100 cm deep, were collected by excavating soil surrounding 45 cm diameter demarcated areas to a depth of 100 cm using a backhoe-outfitted tractor. The column edges were trimmed manually to about 40 cm diameter, the bottom 10 cm was sprayed with a foam sealant, the column encased in a PVC pipe (42.5-cm inside diameter and 110-cm long), following which sodium bentonite and water was added to seal the gap between the soil and the PVC pipe. After setting, the column was cut, wrapped with nylon mesh at the bottom, securely placed on a stainless-steel plate, and transported to a greenhouse facility in Booneville for further experimentation. Each column rested on a stainless-steel grid lysimeter consisting of 100 cells (3.81 cm × 3.81 cm) for collecting leachate draining from the grid cells (Figure 1). Bulk-soil samples from each horizon were also obtained.

Rainwater collected from roof runoff was used for rainfall experiments. Four column leaching experiments were performed: one before applying PL (pre-litter, PLE0), and three experiments (PLE1, PLE2, PLE3) following surface application of PL (moisture content, 14.8%; total P, 14.93 g kg^{-1}) at 5.6 Mg ha^{-1} and rained with an intensity of 3.9 cm h^{-1} for 2-h. The experiment PLE1, followed PL application while PLE2 and PLE3 were performed 8 weeks after PLE1 and were separated by 24 hours.

After a drainage period of 24 hours, leachate samples were weighed and analyzed for dissolved P (DP) and total P (TP) by inductively coupled plasma optical emission spectroscopy (ICP-OES). Dissolved P was analyzed on vacuumed filtered (0.45 μm) samples and TP was determined on unfiltered samples using a nitric acid digestion procedure (APHA, 1995). Particulate P (PP = TP - DP) and P loads (= P concentration × leachate volume) were calculated for each event. Soil P was determined using ICP-OES on filtered (0.45 μm) soil solution extracts using the Mehlich III extractant with a soil-to-extractant ratio of 1:10.

Cropland Data Layer (CDL) values were downloaded for the state of Arkansas for regional estimates of the extent of karst topographies. The CDL values were masked to only include values from areas with karst topography (i.e., "Residuum and Colluvium from Carbonate Rocks"). The mask was generated using rasterized soil data from the "Soil Explorer" Land-use App (available at: https://itunes.

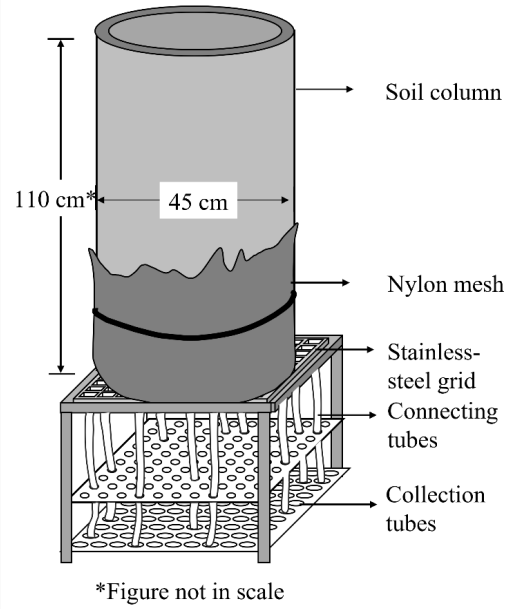

Figure 1: Laboratory set-up of a soil column with a grid sampler with 100 cells each measuring 3.81 cm × 3.81 cm installed at the bottom of the soil column [adapted from Katuwal et al. (2021)].

apple.com/us/app/soil-explorer/id996159565). Total values for each CDL landcover class located on karst topography were summed to calculate total area in hectares of each class. The values were grouped into agricultural or non-agricultural based on CDL categories, and agricultural production areas occurring on karst topographies in Arkansas were used to estimate potential regional P preferential transport.

Total leachate volume, concentrations, and loads of TP, DP, and PP in the leachate were analyzed by ANOVA using PROC GLIMMIX procedure in SAS (SAS V9.4, SAS Institute, 2017), with location (karst and non-karst landscapes) as fixed effects and soil column (replication) a random effect, with irrigation event (i.e., PEL1, PLE2, and PLE3) as a repeated measure. Statistical significance was evaluated at $p = 0.05$ and the means separated using Fisher's least significant difference (LSD) at a Type I error rate of 5%.

Results and Discussion

Soil properties

Soils from both the sites were characterized by argillic horizons (clay contents > 20%) and elevated soil P in the surface horizons (Table 1). Owing to a long history of PL application in the karst landscape, soil P in the A horizon was almost three times that of the non-karst soil. Low soil bulk density for the karst derived soils up to the depth of 73 cm was associated with the high content of rock fragments (Al-Qinna et al., 2014; Katuwal et al., 2021), common in the Clarksville and Nixia soil series of the karst landscape.

Leachate P losses before poultry litter application

Soils from both the sites exhibited a large variability in leachate volumes [coefficients of variation (CV); karst derived soil: 67%, non-karst derived soil: 87%] in PLE0. The variability in TP concentration was less with average leachate TP concentrations of 2.64 and 2.29 mg L^{-1} from karst and non-karst derived soils, respectively. Dissolved P and PP losses accounted for an average of 47 and 53% of TP losses, respectively. The differences in leachate volume ($p = 0.65$), TP ($p = 0.47$), DP ($p = 0.53$), and PP (p

Table 1: Soil properties for the different horizons (Adapted from Katuwal et al., 2021).

Soil	Horizon: Depth (cm)	Bulk density (g cm^{-3})	Sand (%)	Silt (%)	Clay (%)	OC (%)	P (mg kg^{-1})
Karst-derived (Typic Paleudults and Glossic Fragiudults)	A: 0-15	1.29	19.8	68.0	12.2	2.44	405.6
	E: 15-43	1.23	20.2	69.5	10.3	0.48	179.9
	BE: 43-57	1.20	16.7	60.1	23.2	0.45	72.9
	Bt1: 57-73	1.09	17.9	55.6	26.6	0.35	31.0
	Bt2: 73-89	1.62	24.1	49.8	26.1	0.13	1.0
	Bt3: 89-100	1.52	23.1	18.2	58.8	0.2	< 0.2
Non-karst derived (Typic Fragiudults)	A: 0-7	1.22	41.4	50.4	8.2	5.26	144.1
	BE: 7-20	1.70	34.3	46.2	19.5	0.82	23.5
	Bt1: 20-33	1.70	30.2	43.5	26.3	0.45	9.8
	Bt2: 33-49	1.62	27.7	39.7	32.5	0.35	5.8
	2Bt3: 49-77	1.62	30.6	40.7	28.7	0.36	2.4
	2Btg: 77-100	1.53	28.9	38.4	32.8	0.24	0.7

Note: Bulk density of the soil without coarse fragments > 2 mm determined using clod method; OC, organic carbon; P, determined using Mehlich III extractant with a soil-to-extractant ratio of 1:10.

= 0.42) loads were not significant, despite differences in initial soil P concentrations between the two soils (Table 1). Limited time for mobilization of P adsorbed to soil by the fast-flowing water through preferential flow pathways in the karst-derived soils could be associated with similar leachate P concentrations for the two soils.

Leachate P losses after poultry litter application

Initial soil moisture content (v/v) of the surface layer (≈ 7.6 cm) was 34, 15, and 27% before irrigation during PLE1, PLE2, and PLE3, respectively. Variation due to initial soil moisture content was observed in leachate volume ($p = 0.005$) with greater volume in PLE1 than PLE2 and PLE3, but not different between PLE2 and PLE3 (Figure 2). Overall, the leachate volume from the karst derived soil was approximately four times greater ($p = 0.007$) compared to soil from non-karst landscape. No interaction between landscape and irrigation event ($p = 0.33$) was observed (Figure 2).

Average leachate TP concentrations were not different for the two locations ($p = 0.07$, Table 2) and only the main effect of irrigation event was significant ($p = 0.02$). Across both locations, the average TP concentration increased from 2.42 mg L^{-1} in PLE0 to 5.61 mg L^{-1} in PLE1, which decreased to 3.14 and 2.88 mg L^{-1} in PLE2 and PLE3, respectively. Leachate TP mainly consisted of DP averaging 70.4% of TP concentration over all soils and irrigation events.

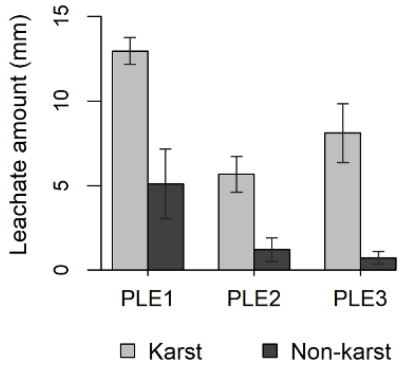

Figure 2: Comparison of leachate amount (mm) among irrigation events following litter application (PLE1, PLE2, and PLE3) from soils from karst and non-karst landscapes. Error bars represent standard errors.

Total leachate P loss from the applied PL varied between the two soils among irrigation events ($p = 0.001$) (Figure 3a). In karst derived soil greater TP leached from PLE1 (0.99 kg ha^{-1}) as compared to PLE2 (0.20 kg ha^{-1}) and PLE3 (0.26 kg ha^{-1}). Average TP loss from non-karst derived soil decreased with the successive irrigation events, however, the difference was not significant. The TP loss from the karst derived soil was almost six times that from the non-karst landscape (Table 2) resulting mostly from the spike in leachate P losses in karst derived soil in PLE1 (Figure 3a). For PLE2 and PLE3 the differences in TP between the two soils were not significant likely due to; first, decline in litter P content after PLE1 combined with the slow transformation rate of stable litter P forms to water extractable forms (Vadas et al., 2007), and second, greater retention of P in the soil because of lower antecedent soil moisture content before PLE2 and PLE3 and consequently lower leachate volume compared to PLE1 in both the soils. In fact, leachate volume during PLE2 and PLE3 from the non-karst derived soil was lower than the PLE0, resulting in lower TP losses as compared to the PLE0.

The contribution of DP to TP loss in both soils decreased with irrigation events, with 85, 63, and 52% in PLE1, PLE2, and PLE3, respectively. In the karst derived soil, leachate DP loss was greater than PP loss in PLE1 whereas in PLE2 and PLE3, DP and PP losses did not significantly differ. In soil from the non-karst landscape, there was no difference between DP and PP for any of the irrigation events (Figure 3b).

Regional estimates of extent of karst topographies

Based on CDL values and the Soil Explorer Land-use App, there are currently 350,846 hectares of karst topography (i.e., Residuum and Colluvium from Carbonate Rocks) under agricultural production in Arkansas. Therefore, assuming 83.63 kg ha^{-1} P applied (i.e., the total P applied in the form of PL) to the 350,846 ha of karst topography in Arkansas, there would be potential for 29,342,756 kg P applied to agricultural fields overlying karst. Given that 1.18% of total P was measured in the leachate from karst columns, this could result in 346,245 kg of P that has

Table 2: Average P concentrations (mg L^{-1}; total P, TP; dissolved P, DP; particulate P, PP) and cumulative P loss in leachate (kg ha^{-1}) after 3 irrigation events (intensity of 3.9 cm hr^{-1} for 2 hours) following poultry litter application (5.6 kg ha^{-1}) in soil columns from karst and non-karst landscapes. Values within parenthesis denote standard error.

Soils	TP conc (mg L^{-1})	DP conc (mg L^{-1})	PP conc (mg L^{-1})	TP load (kg ha^{-1})	DP load (kg ha^{-1})	PP load (kg ha^{-1})
Karst	5.05 (0.81) a†	4.26 (0.67) a	0.79 (0.36) a	1.46 (0.20) a†	1.30 (0.21) a	0.16 (0.03) a
Non-karst	2.82 (0.62) a	1.84 (0.81) a	0.98 (0.37) a	0.22 (0.09) b	0.13 (0.04) b	0.09 (0.08) a

† Different letters denote significant differences ($p < 0.05$) per variable.

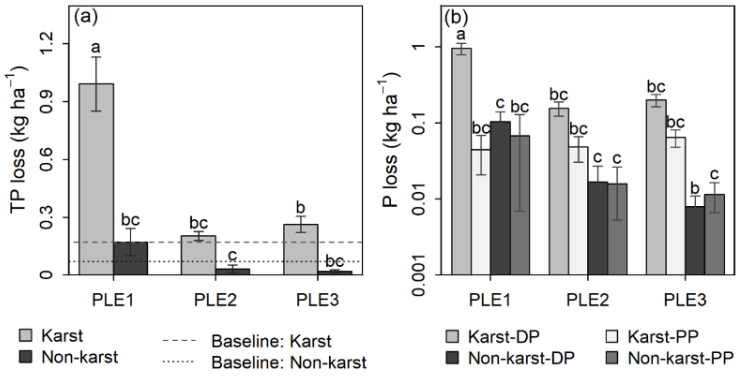

Figure 3. (a) Total phosphorus (TP) loss (kg ha^{-1}) and (b) loss of phosphorus (P loss, kg ha^{-1}) in dissolved (DP) and particulate (PP) forms in leachate during irrigation events following litter application (PLE1, PLE2, and PLE3) from soils from a karst and non-karst landscape. Error bars represent standard errors and different letters denote significant differences at p = 0.05. Broken horizontal lines in the left figure represent leachate TP loss in the irrigation event prior to litter application (pre-litter irrigation, or baseline).

the potential to reach an aquifer given the same rainfall, poultry litter P level, and soil moisture conditions as in this experiment. Identifying nutrient leaching potential estimates in regional karst systems may be useful for inclusion in nutrient management plans and in future state-wide P indices. Such information may allow for precision nutrient management for producers, researchers, and policy decision-makers. Since P leaching was 8 times greater in karst landscapes, it may be more environmentally renumerating on a regional basis to transport high P manure sources to non-karst soils. Further data on the extent of regional karst distribution are needed for model validation and verification to gain greater insight into regional nutrient leaching and potential environmental repercussions for tailoring nutrient management plans based on topography for forage, crop, and livestock producers.

Implications of the study

The results of this study suggest greater P leaching potential from surface-applied PL from 1-m deep soil columns of a karst landscape compared to soil from a non-karst landscape. However, potential impairment of water quality from P leaching in karst landscapes is contingent upon the direct connectivity of PFPs to groundwater. Retention of P in the epikarst layer can reduce the risk of event-driven P losses (Jarvie et al., 2014). Even if P leaching losses may not be a concern for short-term water quality issues, the susceptibility of karst derived soils to deep soil profile leaching may increase P concentration of deeper soil layers over time which may serve as a potential P source once remobilized (Sharpley et al., 2013). Further, elevated soil nutrient and metal concentration can impact water quality even after cessation of PL application (McMullen et al., 2014; Menjoulet et al., 2009).

It is also important to note that this study was performed with a few sets of soils and large-scale extrapolation is cautioned. Previous in-situ studies performed within the mantled karst landscape of NW Arkansas have acknowledged greater content of the chert fragments in the soil layer to be associated with greater hydraulic conductivity and infiltration rates (Al-Qinna et al., 2014; Sauer et al., 2005). The results indicate that the presence of PFPs in combination with other features such as depth of ground water, or presence of perched groundwater may be used to assess P vulnerability to water impairment or at least identify potential hotspots. Such information may allow for precision nutrient management for producers, researchers, and policy decision-makers.

Conclusions

In this study, P loss from surface-applied poultry litter was compared for large intact soil columns derived from a karst and a non-karst landscape under three successive irrigation events. Results indicate that P transport from surface-applied litter through soils is largely determined by the leachate volume and prevalence of karst topographies, where soils developed in karst landscapes may have a greater degree of preferential flow pathways compared to soils from non-karst terrain. Following poultry litter applications, at least six times greater P leached in karst derived soil than from a non-karst landscape. Dissolved P constituted the major fraction (more than 80%) of the total P losses in leachate. In contrast, PP was a minor component of the total P load following surface application of poultry litter. Therefore, the soil layer 1 m above the mantled karst landscape is vulnerable to vertical P transport into deeper soil layers with the potential to increase legacy P and possess a threat to surface and groundwaters.

With currently 350,846 hectares of karst topography under agricultural production in Arkansas and land application of poultry litter to pastures within the region being common, there is high P application potential to agricultural fields overlying karst geologies and thus the incidental transfers of P to deeper soil layers. Identifying vulnerable areas in regional karst systems may be useful for tailoring nutrient management plans based on topography for forage, crop, and livestock producers and in future state-wide P indices.

Acknowledgements

This material is based upon work supported by the

United States Geological Survey under grant agreement No. G21AP10581 and administered by the Arkansas Water Resources Center. The views and conclusions contained in this document are those of the authors and should not be interpreted as representing the opinions or policies of the U.S. Geological Survey.

References

Al-Qinna, M., Scott, H. D., Brye, K. R., Van Brahana, J., Sauer, T. J., & Sharpley, A. (2014). Coarse fragments affect soil properties in a mantled-karst landscape of the ozark highlands. Soil Science, 179(1), 42–50.

Allaire, S. E., van Bochove, E., Denault, J. T., Dadfar, H., Thériault, G., Charles, A., & de Jong, R. (2011). Preferential pathways of phosphorus movement from agricultural land to water bodies in the canadian great lakes basin: A predictive tool. Canadian Journal of Soil Science, 91(3), 361–374.

Jarvie, H. P., Sharpley, A. N., Brahana, V., Simmons, T., Price, A., Neal, C., Lawlor, A. J., Sleep, D., Thacker, S., & Haggard, B. E. (2014). Phosphorus retention and remobilization along hydrological pathways in karst terrain. Environmental Science and Technology, 48(9), 4860–4868.

Jarvis, N. J. (2007). A review of non-equilibrium water flow and solute transport in soil macropores: Principles, controlling factors and consequences for water quality. European Journal of Soil Science, 58(3), 523–546.

Katuwal, S., Ashworth, A. J., & Owens, P. R. (2021). Preferential flow under high-intensity short-duration irrigation events in soil columns from a karst and nonkarst landscape. Vadose Zone Journal, 20(6), e20160.

King, K. W., Williams, M. R., Macrae, M. L., Fausey, N. R., Frankenberger, J., Smith, D. R., Kleinman, P. J. A., & Brown, L. C. (2015). Phosphorus transport in agricultural subsurface drainage: A review. Journal of Environmental Quality, 44(2), 467–485.

Kung, K.-J. S., Steenhuis, T. S., Kladivko, E. J., Gish, T. J., Bubenzer, G., & Helling, C. S. (2000). Impact of preferential flow on the transport of adsorbing and nonadsorbing tracers. Soil Science Society of America Journal, 64(4), 1290–1296.

Mahmood-Ul-Hassan, M., Rashid, M., Akhtar, M. S., & Rafique, E. (2010). Nitrate and phosphate leaching from aridisols and entisols: Laboratory studies and field observations. Soil and Sediment Contamination, 19(3), 261–276.

McMullen, R. L., Brye, K. R., Daigh, A. L., Miller, D. M., Gbur, E. E., Pirani, A. L., Evans-White, M. A., & Mason, R. E. (2014). Long-Term Leachate Water Quality Trends from a Broiler-Litter-Amended Udult in a Karst Region. Vadose Zone Journal, 13(9), vzj2014.06.0064.

Menjoulet, B. C., Brye, K. R., Pirani, A. L., Haggard, B. E., & Gbur, E. E. (2009). Runoff Water Quality from Broiler Litter-Amended Tall Fescue in Response to Natural Precipitation in the Ozark Highlands. Journal of Environmental Quality, 38(3), 1005–1017.

National Ocenic and Atmospheric Administration. (2021). Data Tools: 1981-2010 Normals. Annual/seasonal normals. https://www.ncdc.noaa.gov/cdo-web/datatools/normals

Radcliffe, D. E., Reid, D. K., Blombäck, K., Bolster, C. H., Collick, A. S., Easton, Z. M., Francesconi, W., Fuka, D. R., Johnsson, H., King, K., Larsbo, M., Youssef, M. A., Mulkey, A. S., Nelson, N. O., Persson, K., Ramirez-Avila, J. J., Schmieder, F., & Smith, D. R. (2015). Applicability of models to predict phosphorus losses in drained fields: A review. Journal of Environmental Quality, 44(2), 614–628.

Reid, D. K., Ball, B., & Zhang, T. Q. (2012). Accounting for the risks of phosphorus losses through tile drains in a phosphorus index. Journal of Environmental Quality, 41(6), 1720–1729.

SAS Institute. (2017). SAS 9.4. SAS Institute.

Sauer, T. J., & Logsdon, S. D. (2002). Hydraulic and physical properties of stony soils in a small watershed. Soil Science Society of America Journal, 66(6), 1947–1956.

Sauer, T. J., Logsdon, S. D., Van Brahana, J., & Murdoch, J. F. (2005). Variation in infiltration with landscape position: Implications for forest productivity and surface water quality. Forest Ecology and Management, 220(1–3), 118–127.

Sharpley, A. N., Daniels, M. B., Brye, K. R., VanDevender, K., Burke, J., Berry, L. G., & Webb, P. (2020). Fate and transport of phosphorus-containing land-applied swine slurry in a karst watershed. Agrosystems, Geosciences & Environment, 3(1).

Sharpley, A. N., Jarvie, H. P., Buda, A., May, L., Spears, B., & Kleinman, P. (2013). Phosphorus legacy: Overcoming the effects of past management practices to mitigate future water quality impairment. Journal of Environmental Quality, 42(5), 1308–1326.

Sims, J. T., Simard, R. R., & Joern, B. C. (1998). Phosphorus loss in agricultural drainage: Historical perspective and current research. Journal of Environmental Quality, 27(2), 277–293.

Vadas, P. A., Harmel, R. D., & Kleinman, P. J. A. (2007). Transformations of soil and manure phosphorus after surface application of manure to field plots. Nutrient Cycling in Agroecosystems, 77(1), 83–99.

Williams, M. R., King, K. W., Ford, W., Buda, A. R., & Kennedy, C. D. (2016). Effect of tillage on macropore flow and phosphorus transport to tile drains. Water Resources Research, 52(4), 2868–2882.

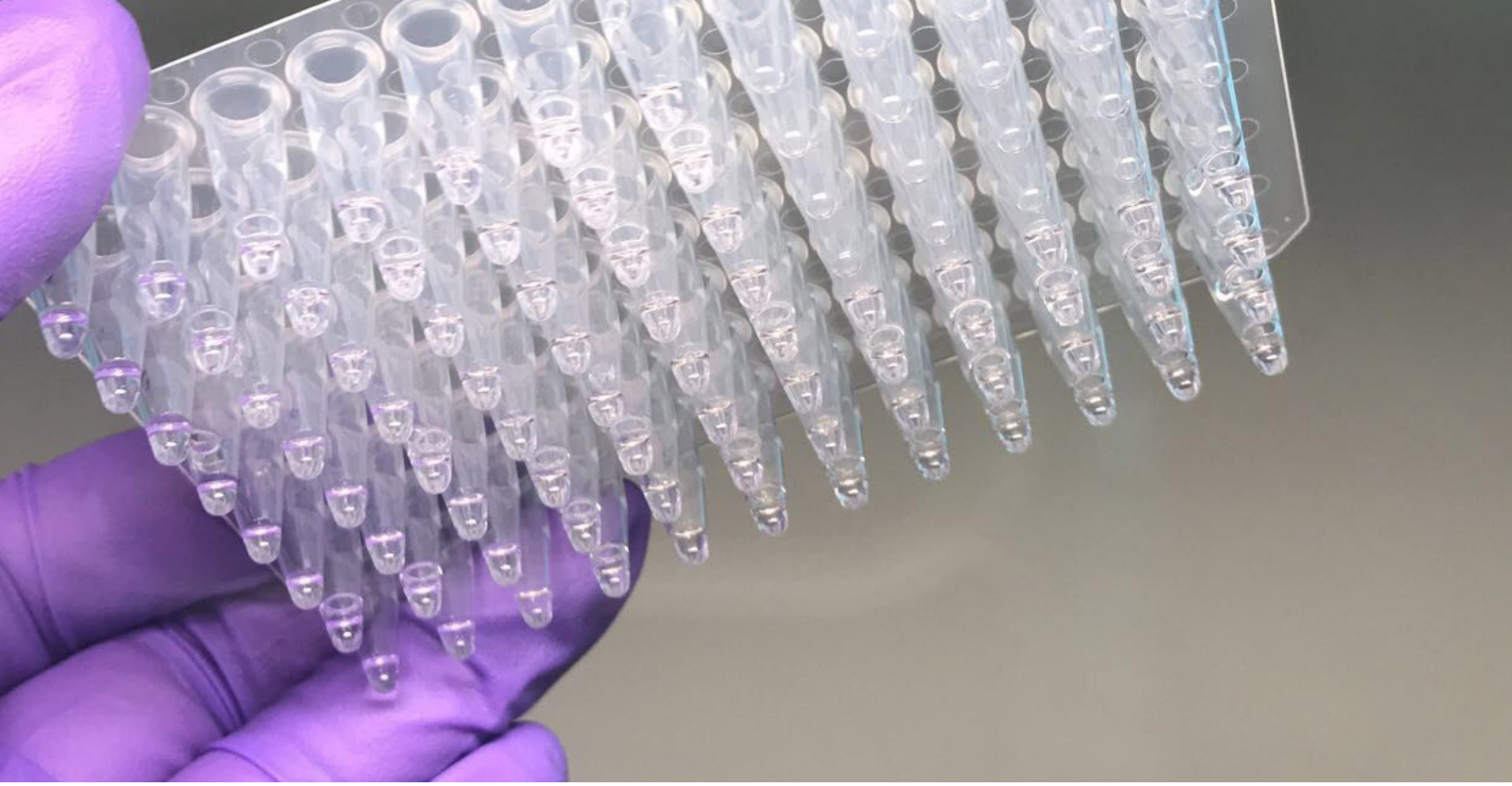

Image caption: 96-well plate used in the qPCR. Each well contains 20 uL of qPCR reaction for SARS-CoV-2 gene target amplification and detection from wastewater samples. Photo courtesy of Aaron Long.

A Snapshot of SARS-CoV-2 Virus in Wastewater Treatment Plants

Aaron Long[1], Katie Loethen[2], Asal Behzadnezhad[1], and Wen Zhang[3]

[1]Graduate Student, Department of Civil Engineering, University of Arkansas, Fayetteville, AR 72701; [2]Undergraduate Student, Department of Biological Engineering, University of Arkansas, Fayetteville, AR 72701; [3]Associate Professor, Department of Civil Engineering, University of Arkansas, Fayetteville, AR 72701

Abstract: The Severe Acute Respiratory Syndrome Coronavirus 2 (SARS-CoV-2) can spread the viral RNA in wastewater by the feces of those experience COVID-19 symptoms. While wastewater monitoring of SARS-CoV-2 in the raw sewage has been confirmed as an effective tool to predict COVID-19 infection, the goal of this study is to assess the presence of SARS-CoV-2 throughout various wastewater treatment processes. Wastewater samples were collected from wastewater treatment plants (WWTPs) in the state of Arkansas from August 2020 to June 2021 and measured for the relative concentration of SARS-CoV-2 using RT-qPCR. The SARS-CoV-2 concentrations in the raw sewage measured in this study are similar to other published studies, targeting the N1 and N2 genes of the virus. The virus concentration was measured after each wastewater treatment step within WWTPs, including primary sedimentation, activated sludge, filtration and disinfection. Results show the majority of the virus removal occurred in the secondary treatment (activated sludge), while the primary sludge could serve as a potential source for the virus. The virus was only occasionally detected after disinfection (chlorination or UV disinfection). Overall, WWTPs can remove the SARS-CoV-2 virus at an average of 98.7%, while complete removal was achieved on 82% of the sampling days. Further investigation is required to ensure complete virus removal from wastewater such as improving existing treatment process or supplementing with additional treatment steps. The state of Arkansas and other regions can directly use the results to assess the performance of their WWTPs regarding virus removal, and make informed decisions to improve the effluent quality.

Key Points:

- This study measured SARS-CoV-2 virus concentration throughout wastewater treatment.
- Virus concentration in raw sewage fluctuated over time using N1 and N2 primers.
- SARS-CoV-2 virus was only occasionally detected in treated wastewater effluent.
- Secondary treatment (activated sludge) removes the majority of SARS-CoV-2 virus.

Introduction

Severe Acute Respiratory Syndrome Coronavirus 2 (SARS-CoV-2) is the virus that causes COVID-19, and has infected 265 million globally and killed over 780,000 individuals in the United States as of December 2021. The main transmission routes of COVID-19 are through respiratory droplets and direct contacts. However, recent evidence showed the ACE2 protein can act as a cell receptor for the SARS-CoV-2 virus, which is abundantly expressed in the glandular cells of gastric, duodenal, and rectal epithelia in humans (Xiao et al., 2020). Significant shedding of the SARS-CoV-2 virus can be found in fecal samples, regardless of diarrhea. Several studies have detected the viral RNA fragments in COVID-19 patients' fecal matter throughout their illness and after recovery (Holshue et al., 2020; Xiao et al., 2020). As a result, the viral RNA can be found in domestic wastewater treatment plants (WWTPs), where the sewage is subjected to a series of treatment processes.

Typical WWTPs are designed to remove solids, nutrients and pathogens by sedimentation, activated sludge and disinfection. Various regulations exist to govern the wastewater effluent discharge. In the United States, National Pollutant Discharge Elimination System (NPDES) permits are required for facilities that release treated waste into waters of the state. Even though Enterococci or fecal coliforms in the effluent are required for routine testing by most states, no limits on viruses are included in these permits. Since WWTPs are not specifically designed for virus removal, certain viruses can pass through the treatment processes and enter the environment through effluent discharge, including the SARS-CoV-2 virus (Rimoldi et al., 2020).

Previous studies have focused on the fate of viruses throughout WWTPs such as SARS-CoV-1 (Wang, Li et al. 2005, Wang, Li et al. 2005), pepper mild mottle virus (PMMoV), tobacco mosaic virus (TMV) (Tandukar et al., 2020), and Adenovirus (Hata, Kitajima et al. 2013). Currently there is no report indicating the COVID-19 infection through wastewater effluent. However, the fate of this virus in wastewater treatment deserves attention to ensure that WWTPs do not become a source of such contamination.

As a result, the objective of this study is to investigate the presence of the SARS-CoV-2 virus within wastewater treatment processes. Real wastewater at the influent and after each treatment step was collected from several WWTPs during the COVID-19 pandemic and analyzed for the viral RNA concentration using reverse transcription quantitative polymerase chain reaction (RT-qPCR). The removal efficiency was compared based on treatment levels. The results can be used by facilities and regulatory agencies to determine if the SARS-CoV-2 in wastewater poses a threat to the receiving water bodies and the communities, and if additional treatment is required to eliminate the concern.

Methods

From August 2020 to June 2021, 663 wastewater samples were collected from 14 WWTPs in northwest and central Arkansas, including Paul R. Noland and Westside (Fayetteville), Springdale, Rogers, P Street and Massard (Fort Smith), West Fork, Prairie Grove, Adams Field and Little Maumelle and Fourche Creek (Little Rock), Pine Bluff, Tupelo Bayou and Tucker Creek WWTPs (Conway), and a Washington County Lift Station (named WCPOID5). Raw sewage samples were collected from all WWTPs mentioned above. Treated wastewater samples were also collected from WWTPs in Fayetteville and Little Rock, including post primary clarification, post secondary clarification, post filtration (if available), and post disinfection (final effluent). The majority of samples collected were composite samples, with occasional grab samples collected. 250 mL of wastewater were collected at each location at a semiweekly frequency during the sampling period and stored in HDPE bottles (VWR, Radnor, PA). The sample bottles were sealed in individual Ziploc bags and placed in foam coolers with ice packs after collection. The samples were then transported from WWTPs to the University of Arkansas research laboratory on the same day of collection.

Proper personal protective equipment (PPE) was used for handling the wastewater including KN95 face masks, face shields, disposable lab coats, and nitrile gloves. 70% ethanol was sprayed on work surfaces to disinfect before and after sample processing. Upon arrival at the research laboratory, 140 µL of wastewater was extracted for RNA using direct extraction using the QIAamp Viral RNA Mini Kit (Qiagen, Germantown, MD) following the manufacturer's recommended protocol. Sixty µL of RNA extracts were yielded from the extraction and stored in -80°C until the subsequent qPCR process.

The relative concentration of SARS-CoV-2 virus was quantified using RT-qPCR on a Bio-Rad CFX Connect system following the Master Mix protocol recommended by the CDC. Each 20-µL reaction consists of 8.5 µL of nuclease-free water, 1.5 µL of prime/probe mix, 5 µL of RNA extracts and 5 µL of Reliance One-Step Multiplex Supermix (Bio-Rad, Hercules, CA). The plasmid controls and primer/probes for N1, N2 and RP genes (included within the 2019-CoV Plasmid Controls and 2019-nCoV CDC RUO qPCR Probe Assay) were purchased from IDTDNA (Coralville, IA). Detection with either N1 or N2 indicates the presence of SARS-CoV-2 virus, and RP gene that targets human RNase P gene for detection of human nucleic

acids was included as a positive control for sample integrity. The thermal cycling protocol followed the Bio-Rad Reliance One-Step Multiplex Supermix instructions for 20-µL reactions at 50°C for 10 min and 95°C for 10 min, followed by 40 cycles of 95°C for 10s and 60°C for 30s. For PCR quality control, duplicate 5-point standard curves for N1, N2 and RP genes and negative controls were included for each plate run. Standard curves with an $R^2 \geq 0.98$ were considered acceptable.

Duplicate RNA extracts were included for each gene target in RT-qPCR (e.g., one influent sample had duplicate wells for N1 and the same for N2). If detection occurred in both wells, a mean value and standard deviation was calculated. If only one well had detection, this value was used to represent the concentration for that sample. The samples shown no detection in both N1 and N2 were considered zero in virus concentration, following multiple studies that assumed zero concentration for samples below the detected limit to calculate the removal percentages (Wang, Li et al. 2005, Randazzo, Truchado et al. 2020, Kumar, Kuroda et al. 2021, Tran, Le et al. 2021).

A paired t-test was used to analyze the difference of each gene target between two treatment stages (e.g., influent versus primary effluent; primary effluent versus secondary effluent) using both absolute concentrations (gene copy/mL) and percent concentrations relative to the influent (%). A zero effluent concentration on certain days with detectable influent leads to complete virus removal (100%). The statistical analysis shows a significant difference between two treatment stages when $p < 0.05$.

Results and Discussion

SARS-CoV-2 in raw sewage

Figure 1 shows the concentration of SARS-CoV-2 virus using both N1 and N2 in the raw sewage from all treatment plants sampled between 9/2/2020 and 5/10/2021. The range of raw sewage concentration is approximately 1×10^2 to 1×10^5 gene copies/mL (2.86×10^2 to 3.25×10^4 for N1 and 8.09×10^2 to 7.61×10^4 for N2). The concentration range detected by this study is similar to reported values in other SARS-CoV-2 studies outside the United States, including France (Wurtzer, Marechal et al. 2020), Israel (Ali, Yaniv et al. 2021), the Netherlands (Medema, Heijnen et al. 2020), and Spain (Randazzo, Truchado et al. 2020). In addition, the concentration is comparable to other viruses in the raw sewage, including non-enveloped viruses such as adenoviruses ($\leq10^5$ gene copies/mL) and enteroviruses ($\leq10^3$ gene copies/mL) (Wigginton, Ye et al. 2015), or enveloped viruses such as Influenza A (H1N1) (10^2 gene copies/mL) (Heijnen and Medema 2011).

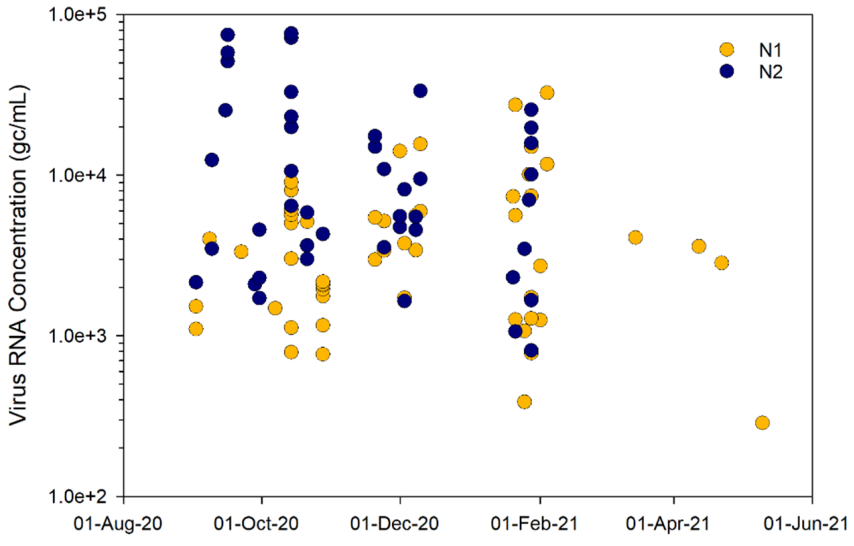

Figure 1: The concentration of SARS-CoV-2 virus in the raw sewage (gene copies/mL)

Between March and June 2021, the COVID case numbers dropped below 200 per day and around 50 daily confirmed cases for the state of Arkansas and the Washington County, respectively (Times). During this time, 148 out of 153 samples from all stages (86 out of 90 raw sewage samples) showed no virus detection. Other studies reported virus detection in wastewater at different infection levels. For example, Mexico showed detection when the area of study had 10-34 daily new cases (Mahlknecht, Reyes et al. 2021); Japan reported detection at 0.0004-0.04% of infected study area (Haramoto, Malla et al. 2020).

SARS-CoV-2 in treated sewage

In addition to raw sewage, wastewater samples after each treatment step within WWTPs in Fayetteville and Little Rock were also collected and analyzed. Figure 2 shows the concentration of SARS-CoV-2 virus throughout four WWTPs in samples taken from 8/9/2020 to 6/3/2021. On each sampling day that had positive detection of the virus in the raw sewage, the virus concentration at each treatment step was normalized using the raw sewage concentration, and an average percentage for each treatment step over the sampling period is presented. The error bars represent the standard deviations of the detected concentration percentage at each treatment step. Primary effluent in three plants showed large standard deviations, indicating significant concentration variations over the sampling period.

Figure 2A shows the data from Noland WWTP in Fayetteville, which has an average daily flow of 12.6 MGD, and the treatment train consists of primary sedimentation, activated sludge, filtration and ozonation. Out of the 111 samples taken

during this period (including raw and treated sewage), 24 samples taken on 13 days had positive measurements of the virus. For N1, the average concentrations were 131.7%, 0.114%, and 4.764% and zero in the primary effluent, secondary effluent, filter effluent, and final effluent respectively. For N2, the virus was only present in the influent and primary effluent, at 100.0% and 40.08% respectively. No virus was detected in the final effluent using N1 or N2.

Figure 2B shows the concentration of SARS-CoV-2 virus throughout the Westside WWTP, which has an average daily flow of 10 MGD, and the treatment train consists of primary sedimentation, activated sludge, filtration, and UV disinfection. Out of the 93 samples taken during this period (including raw and treated sewage), 23 samples taken on 12 days had positive measurements of the virus. For N1, the virus was present in the influent, primary effluent, and secondary effluent at 100.0%, 66.89% and 0.289% respectively. For N2, the virus was only present in the influent and primary effluent, at 100.0% and 149.9% respectively. No virus was detected in the filter effluent or final effluent using N1 or N2.

Figure 2C shows the concentration of SARS-CoV-2 virus throughout the Adams Field WWTP in Little Rock, which has an average daily flow of 36 MGD, and the treatment train consists of primary sedimentation, activated sludge, and UV disinfection. Out of the 13 samples taken during this period (including raw and treated sewage), 8 samples taken on 4 days had positive measurements of the virus. For N1, the virus was present in the influent, primary effluent, secondary effluent, and final effluent at 100.0%, 74.00%, 71.10%, and 29.48% respectively. For N2, the virus was present in the influent, primary effluent, secondary effluent, and final effluent at 100.0%, 81.65%, 8.23%, and 1.16% respectively.

Figure 2D shows the concentration of SARS-CoV-2 virus throughout the Fourche Creek WWTP in Little Rock, which has an average daily flow of 16 MGD, and the treatment train consists of primary sedimentation, activated sludge, and chlorination. Out of the 16 samples taken during this period (including raw and treated sewage), 7 samples taken on 5 days had positive measurements of the virus. For N1, the average concentrations were 100%, 75.7%, and 0.46% in the influent, primary effluent, and final effluent, respectively. The virus was not detected in the secondary effluent for N1. For N2, the virus was present in the influent and primary effluent, at 100.0% and 114.3% respectively. The virus was not detected in the secondary effluent and final effluent for N2.

The virus concentration was compared between treatment stages for both N1 and N2 gene target. There was no significant difference between influent and primary effluent ($p = 0.75$ for N1 and $p = 0.89$ for N2), nor between secondary and final effluent ($p = 0.25$ for N1 and $p = 0.37$ for N2). However, secondary treatment showed effective removal as the virus concentration in primary and secondary effluent differed significantly ($p = 0.0019$ for N1 and $p = 0.018$ for N2).

In addition to the data shown in Figure 2, occasionally the virus was detected in the treated samples without the detection in raw sewage. These samples include Noland plant: 8/20/2020 final effluent (N2), 1/25/2021 primary effluent (N2), and 3/24/2021 primary effluent (N1); Westside plant: 12/1/2020 primary effluent (N1); Little Rock-Adams Field plant: 1/21/2021 primary effluent and

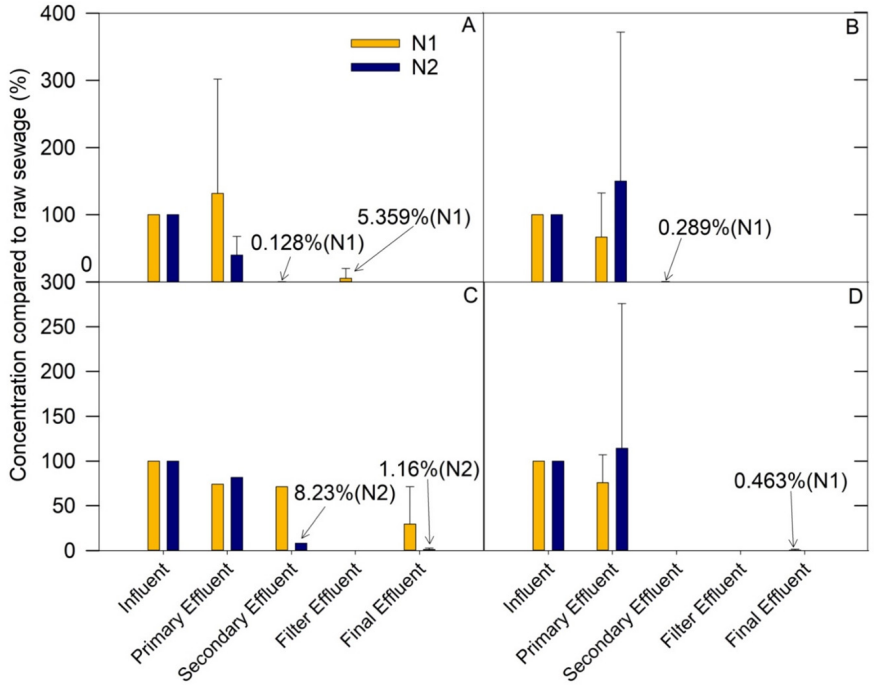

Figure 2: (left) The concentration of SARS-CoV-2 virus throughout treatment stages of different WWTPs in Fayetteville, AR. A: Noland WWTP in Fayetteville, AR. The error bars show the standard deviation from N1: primary effluent (n = 10), secondary effluent (n = 8), and filter effluent (n = 8); & from N2: primary effluent (n = 7) samples. B: Westside WWTP in Fayetteville, AR. The erro r bars show the standard deviation from N1: primary effluent (n = 10) and secondary effluent (n = 10); & from N2: primary effluent (n = 8) samples. C: Adams Field WWTP in Little Rock, AR. The error bars show the standard deviation from N1: final effluent (n = 2); & from N2: final effluent (n = 2) samples. D: Fourche Creek WWTP in Little Rock, AR. The error bars show the standard deviation from N1: primary effluent (n = 2) and final effluent (n = 5); & from N2: primary effluent (n = 2) samples. (Note: C and D do not have filter effluent samples)

secondary effluent (N1). If detected, the concentration in secondary and final effluent were close to the lowest detected concentration. 63 out of 68 secondary and 83 out of 86 final effluent (post-disinfection) samples showed no detection of the virus. One possible reason for virus detection in the treated wastewater but not in raw sewage, is the SARS-CoV-2 virus adsorption to solids in the sludge. Several studies indicate WWTPs could harbor the virus in primary or secondary sludge (Wigginton, Ye et al. 2015, Peccia, Zulli et al. 2020, Serra-Compte, Gonzalez et al. 2021). The detection might come from viral particles disassociated from the sludge within primary or secondary treatment rather than the influent.

Conclusions

Wastewater samples were collected from WWTPs in Arkansas from August 2020 to June 2021 and measured for the relative concentration of SARS-CoV-2 using RT-qPCR. The SARS-CoV-2 concentrations in the raw sewage measured in this study were similar to other published studies, targeting the N1 and N2 genes of the virus. The virus removal after each wastewater treatment step was also studied, including primary sedimentation, activated sludge, filtration and disinfection. Results show the virus removal mainly occurred in the secondary treatment (activated sludge), while the primary sludge could serve as a potential source for the virus. The virus was only occasionally detected after disinfection (chlorination or UV disinfection). Overall, WWTPs can remove the SARS-CoV-2 virus at an average of 98.7%, while complete removal was achieved on 82% of the sampling days. The state of Arkansas and other regions can directly use the results to assess the performance of their WWTPs regarding virus removal, and make informed decisions to improve the effluent quality.

Acknowledgements

This material is based upon work supported by the United States Geological Survey under grant agreement No. G21AP10581 and administered by the Arkansas Water Resources Center. The views and conclusions contained in this document are those of the authors and should not be interpreted as representing the opinions or policies of the U.S. Geological Survey.

References

Ali, H., K. Yaniv, E. Bar-Zeev, S. Chaudhury, M. Shagan, S. Lakkakula, Z. Ronen, A. Kushmaro and O. Nir (2021). "Tracking SARS-CoV-2 RNA through the Wastewater Treatment Process." Acs Es&t Water 1(5): 1161-1167.

Haramoto, E., B. Malla, O. Thakali and M. Kitajima (2020). "First environmental surveillance for the presence of SARS-CoV-2 RNA in wastewater and river water in Japan." Science of the Total Environment 737.

Hata, A., M. Kitajima and H. Katayama (2013). "Occurrence and reduction of human viruses, F-specific RNA coliphage genogroups and microbial indicators at a full-scale wastewater treatment plant in Japan." Journal of Applied Microbiology 114(2): 545-554.

Heijnen, L. and G. Medema (2011). "Surveillance of Influenza A and the pandemic influenza A (H1N1) 2009 in sewage and surface water in the Netherlands." Journal of Water and Health 9(3): 434-442.

Holshue, M., C. DeBolt, S. Lindquist, K. Lofy, J. Wiesman, H. Bruce, C. Spitters, K. Ericson, S. Wilkerson, A. Tural, G. Diaz, A. Cohn, L. Fox, A. Patel, S. Gerber, L. Kim, S. Tong, X. Lu, S. Lindstrom, M. Pallansch, W. Weldon, H. Biggs, T. Uyeki, S. Pillai and W. S.-n. C. Invest (2020). "First Case of 2019 Novel Coronavirus in the United States." New England Journal of Medicine 382(10): 929-936.

Kumar, M., K. Kuroda, M. Joshi, P. Bhattacharya and D. Barcelo (2021). "First comparison of conventional activated sludge versus root-zone treatment for SARS-CoV-2 RNA removal from wastewaters: statistical and temporal significance." Chemical Engineering Journal 425: 130635.

Mahlknecht, J., D. Reyes, E. Ramos, L. Reyes and M. Alvarez (2021). "The presence of SARS-CoV-2 RNA in different freshwater environments in urban settings determined by RT-qPCR: Implications for water safety." Science of the Total Environment 784.

Medema, G., L. Heijnen, G. Elsinga, R. Italiaander and A. Brouwer (2020). "Presence of SARS-Coronavirus-2 RNA in Sewage and Correlation with Reported COVID-19 Prevalence in the Early Stage of the Epidemic in The Netherlands." Environmental Science & Technology Letters 7(7): 511-516.

Peccia, J., A. Zulli, D. Brackney, N. Grubaugh, E. Kaplan, A. Casanovas-Massana, A. Ko, A. Malik, D. Wang, M. Wang, J. Warren, D. Weinberger, W. Arnold and S. Omer (2020). "Measurement of SARS-CoV-2 RNA in wastewater tracks community infection dynamics." Nature Biotechnology 38(10): 1164-+.

Randazzo, W., P. Truchado, E. Cuevas-Ferrando, P. Simon, A. Allende and G. Sanchez (2020). "SARS-CoV-2 RNA in wastewater anticipated COVID-19 occurrence in a low prevalence area." Water Research 181.

Rimoldi, S. G., F. Stefani, A. Gigantiello, S. Polesello, F. Comandatore, D. Mileto, M. Maresca, C. Longobardi, A. Mancon and F. Romeri (2020). "Presence and infectivity of SARS-CoV-2 virus in wastewaters and rivers." Science of the Total Environment 744: 140911.

Serra-Compte, A., S. Gonzalez, M. Arnaldos, S. Berlendis, S. Courtois, J. Loret, O. Schlosser, A. Yanez, E. Soria-Soria, M. Fittipaldi, G. Saucedo, A. Pinar-Mendez, M. Paraira, B. Galofre, J. Lema, S. Balboa, M. Mauricio-Iglesias, A. Bosch, R. Pinto, I. Bertrand, C. Gantzer, C. Montero and X. Litrico (2021). "Elimination of SARS-CoV-2 along wastewater and sludge treatment processes." Water Research 202.

Tandukar, S., S. Sherchan and E. Haramoto (2020). "Applicability of crAssphage, pepper mild mottle virus, and tobacco mosaic virus as indicators of reduction of enteric viruses during wastewater treatment." Scientific Reports 10(1).

Times, T. N. Y. Tracking Coronavirus in Washington County, Arkansas.

Tran, H. N., G. T. Le, D. T. Nguyen, R.-S. Juang, J. Rinklebe, A. Bhatnagar, E. C. Lima, H. M. Iqbal, A. K. Sarmah and H.-P. Chao (2021). "SARS-CoV-2 coronavirus in water and wastewater: A critical review about presence and concern." Environmental research 193: 110265.

Wang, X.-W., J.-S. Li, T.-K. Guo, B. Zhen, Q.-X. Kong, B. Yi, Z. Li, N. Song, M. Jin and W.-J. Xiao (2005). "Concentration and detection of SARS coronavirus in sewage from Xiao Tang Shan Hospital and the 309th Hospital." Journal of virological methods 128(1-2): 156-161.

Wang, X., J. Li, T. Guo, B. Zhen, Q. Kong, B. Yi, Z. Li, N. Song, M. Jin, X. Wu, W. Xiao, X. Zhu, C. Gu, J. Yin, W. Wei, W. Yao, C. Liu, J. Li, G. Ou, M. Wang, T. Fang, G. Wang, Y. Qiu, H. Wu, F. Chao and J. Li (2005). "Excretion and detection of SARS coronavirus and its nucleic acid from digestive system." World Journal of Gastroenterology 11(28): 4390-4395.

Wang, X., J. Li, M. Jin, B. Zhen, Q. Kong, N. Song, W. Xiao, J. Yin, W. Wei, G. Wang, B. Si, B. Guob, C. Liu, G. Ou, M. Wang, T. Fang, F. Chao and J. Li (2005). "Study on the resistance of severe acute respiratory syndrome-associated coronavirus." Journal of Virological Methods 126(1-2): 171-177.

Wigginton, K., Y. Ye and R. Ellenberg (2015). "Emerging investigators series: the source and fate of pandemic viruses in the urban water cycle." Environmental Science-Water Research & Technology 1(6): 735-746.

Wurtzer, S., V. Marechal, J. Mouchel, Y. Maday, R. Teyssou, E. Richard, J. Almayrac and L. Moulin (2020). "Evaluation of lockdown effect on SARS-CoV-2 dynamics through viral genome quantification in waste water, Greater Paris, France, 5 March to 23 April 2020." Eurosurveillance 25(50): 38-44.

Xiao, F., M. Tang, X. Zheng, Y. Liu, X. Li and H. Shan (2020). "Evidence for Gastrointestinal Infection of SARS-CoV-2." Gastroenterology 158(6): 1831.

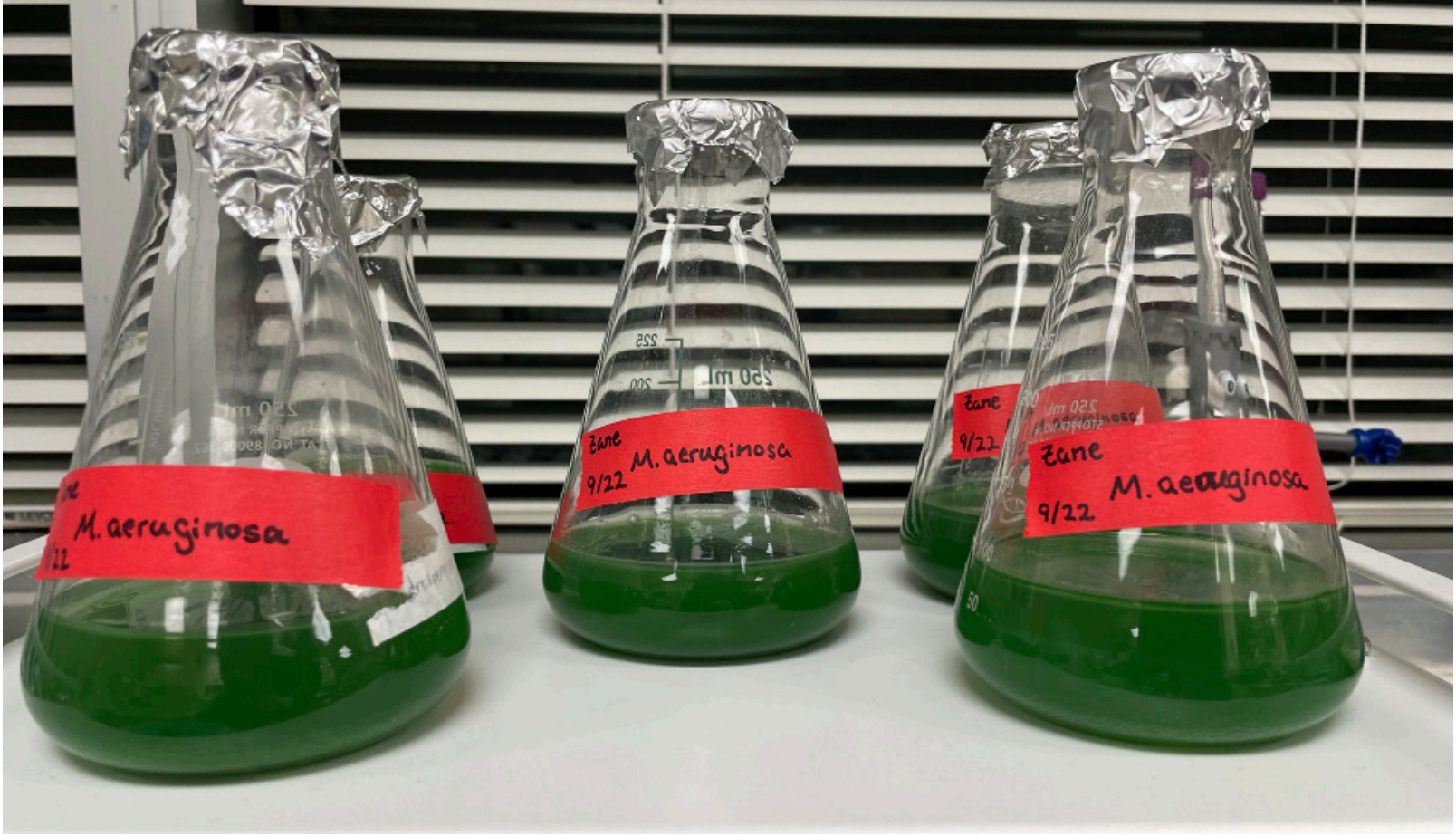

Image caption: Cultures of Microcystis aeruginosa used to conduct these experiments. They are happily fed, awaiting the next experiment. Photo courtesy of Zane Wood.

Assessing Photocatalytic Net for In Situ Harmful Algal Bloom Mitigation

Zane Wood[1] and Wen Zhang[2]

[1]Graduate student, Department of Civil Engineering, University of Arkansas, Fayetteville, AR 72701, [2]Associate Professor, Department of Civil Engineering, University of Arkansas, Fayetteville, AR 72701

Abstract: Harmful algal blooms (HABs) and their associated cyanotoxins cause negative environmental, water quality, and human health impacts. No treatment approach currently exists that can treat both HAB cyanobacteria and cyanotoxins without a pump-and-treat requirement, constant chemical dosage, or possible negative environmental impacts. The objective of this research is to assess the effectiveness of a photocatalytic net for the removal of both cyanobacteria and cyanotoxins with both simulated HAB and real water samples. The photocatalytic net has been designed to be reusable and retrievable from surface waters and contains the non-toxic photocatalyst titanium dioxide (TiO_2). The TiO_2 nanoparticles both in suspension and immobilized form were effective in degrading the most common cyanotoxin microcystin LR (MC-LR) in deionized water. The suspended TiO_2 nanoparticles promote flocculation of cyanobacteria, while the TiO_2 net was unable to remove cyanobacteria biomass. The TiO_2 nanoparticles was unable to degrade MC-LR in lake water due to the presence of other constituents. In conclusion the proposed TiO_2 net will not be a viable option for treating HAB in situ. However, TiO_2 nanoparticles could be applied as a polishing step to remove cyanotoxin from drinking water due to their effectiveness toward degrading MC-LR. This could be further explored by drinking water facilities when the water quality is challenged by HAB in the source water all over Arkansas and other states.

Key Points:

- The TiO_2 nanoparticles both in suspension and on nets were effective in degrading the most common cyanotoxin microcystin LR (MC-LR) in deionized water.
- The suspended TiO_2 nanoparticles promote flocculation of cyanobacteria, while the TiO_2 net was unable to remove cyanobacteria biomass.
- The TiO_2 nanoparticles was unable to degrade MC-LR in lake water due to the presence of other contaminants. However, the treatment could be applied as a polishing step to remove cyanotoxin from drinking water.

Introduction

Harmful algal blooms (HABs) produce biomass and cyanotoxins that adversely impact the health of humans, livestock, and wildlife through altered water quality, nutrient availability, and environmental quality (Anderson, Glibert et al. 2002). An estimated 25 to 75% of HAB cyanotoxins, such as microcystin-LR, are toxic (Blaha et al., 2009; Meng et al., 2015). Cyanobacteria have negative impacts on ecosystem function and adversely impact human health, with outcomes including liver damage, immunotoxicity, and neurotoxicity (Blaha et al., 2009; Marsalek et al., 2012). Arkansas is directly affected by HABs, with the mortality of certain types of catfish located in Mississippi, Alabama, Arkansas, and Louisiana ponds occurring within 24 hour of microcystin-LR poisoning (Zimba et al., 2001). Given the prevalence and importance of surface waters in the state of Arkansas for human recreation, environmental health, fresh water supply, and municipal/industrial development, the occurrence of HABs has a direct impact on Arkansas state economic vibrancy and environmental health.

Annually, the U.S. alone spends $2.2-4.6B on methods, including chemical treatment, flocculation, coagulation, or sedimentation, to battle the effects of HABs (Marsalek et al., 2012; Meng et al., 2015; Meglic et al., 2017; Yang et al., 2018; Zhou et al., 2018). However, these methods have key disadvantages including cost, repeat treatment, chemicals handling, detrimental environmental impacts, and inefficiency (Marsaleket al., 2012). Currently there are no effective and sustainable treatment methods for in situ simultaneous treatment of cyanobacteria and cyanotoxins.

In our initial work on this project, we have designed, fabricated, and tested a photocatalytic net for localized, in situ treatment of HABs by immobilizing titanium dioxide (TiO_2) nanoparticles on nylon fiber nets. The net technology would allow mitigation of both HABs and cyanotoxins in a contaminated water source, where the net is intended to be reusable and retrievable. The local application of a net at the HAB/cyanotoxin source would prevent the spread of HAB/cyanotoxin and would minimize unwanted catalytic reactions, resulting in point-source treatment with few negative side effects. We have recently demonstrated that our photocatalytic net design is successful at degrading a cyanotoxin, microcystin-LR (MC-LR) in synthetic water samples. A comparison to control experiments performed either without UV light or without the presence of the photocatalyst (TiO_2 NPs) has confirmed that our net design does in fact degrade MC-LR and that the TiO_2 NP photocatalyst is key to degradation in the presence of UV light. The objective of this research is to assess the effectiveness of the photocatalytic net for the removal of both cyanobacteria and cyanotoxins with both simulated HAB and real water samples.

The proposed research activities will allow our team to demonstrate net performance in real water and in situ outdoor scenarios. In addition, our results will demonstrate the role of cyanobacteria and toxin concentration(s) on the net effectiveness as well as identify areas for future fundamental and applied research on materials science, toxin degradation pathway, and understanding microorganism/toxin dynamics. This work directly corresponds to the Arkansas Water Resources Center's (AWRC) research areas of interest (HABs), and will benefit environmental quality and technology-based economic development for the State of Arkansas and the goals of the AWRC through the development of better mitigation strategies for HABs and by supporting the education and research of the funded graduate students.

Methods

Cyanobacterial culture of Microcystis aeruginosa was obtained from UTEX laboratories at the University of Austin, Texas. Each culture was maintained in 125 mL glass Erlenmeyer flasks by an open window to encourage natural photosynthesis and were fed every 21 days with BG – 11 medium. The flasks were covered with caps made from cotton balls and aluminum foil to facilitate gas exchange and avoid contamination. The cyanobacteria growth was tracked by measuring optical density (OD) on a spectrophotometer at a wavelength of 680 nm, and cell morphology was checked regularly using a Nikon Ni-E microscope.

Prior to each experiment, 50 mL of the cyanobacteria culture was centrifuged at 5000 rpm for 5 minutes and the supernatant discarded to remove contamination. The cell pellet accumulated after centrifugation was then re-suspended into 75 mL of BG-11 solution. All experiments were carried out in 125 mL Erlenmeyer flasks and placed inside the shaker at 100 rpm through the duration of the experiment. Both the stock solution of suspended TiO_2 (5 g/L) and TiO_2-sprayed nets were obtained from Dr. Greenlee's research laboratory. Briefly, a 1:6 mass ratio Nafion to TiO_2 methanol solution was made by diluting and mixing concentrated TiO_2 nanoparticles and concentrated Nafion ionomer with methanol. Woven, 100 μm hole nylon mesh was cut into 4 cm by 4 cm squares and encased in aluminum foil on all sides but the front. Airbrush tubing was connected to an air supply, which was turned on to a constant and consistent airflow. A 250 μL volume of 1:6 mass ratio Nafion to TiO_2 methanol solution was added to the fluid cup, and a coat of the solution was applied evenly onto the surface of the nylon net. Additional spray coats of solution were applied once a previous coat dried for approximately 2 minutes and was dry to the touch. Nylon

nets were spray coated 5 times with TiO_2 and Nafion solution. Spray coated nets were left overnight in a hood to dry completely before experiments.

For suspended TiO_2 experiments, 1 mL of suspended TiO_2 nanoparticles were added to 40 mL of cyanobacteria in BG-11 medium to reach a final NP concentration of 0.25 g/L. UV light was placed 2 inches away from the flasks. Liquid samples are taken at the start of the experiment, and then every 30 minutes after the first hour of treatment. The experiments have ranged in duration from 120 minutes to 24 hours. 20 µL of samples were measured on the Coulter counter to determine the particle distribution. Another 20 µL samples are also taken at the beginning, middle and end of the experiment to observe any changes in cell morphology under the microscope. For UV treated flasks, the UV-light was on for 8 hours each day until the end of the experiment.

For TiO_2 net experiments, the set up was similar to the suspended NP experiment, only the suspended NP was replaced by the sprayed nets. The nets were placed into the flasks using clean tweezers at the beginning of the experiment, and the duration of the experiment ranges from 3 to 72 hours. The nets are retrieved from the flasks at the end of the experiment and placed into petri dishes for observation under the microscope. Samples were taken at the same frequency for particle and microscopy analysis.

All 20 µL samples for coulter counter measurements were diluted in 10 mL of previously filtered ISOTON II dilutant before running it through the Coulter counter. ISOTON II used to dilute the samples was filtered through a 0.2 µm diameter filter. 100 µm of aperture tube was used to capture particles ranging from 2 to 60 µm. For each measurement, 75 µL of samples were taken into the Coulter counter and particle distribution was reported. For microscopy, samples were placed on microscope glass slides and then covered with a glass slide cover. The samples were then observed under the 20x objective using light microscopy mode. Samples pictures were then taken using the Nikon-NIS program.

Real water samples (1-2 L) from Lake Fayetteville were obtained throughout the spring and summer months of 2021 through collaboration with Dr. Brian Haggard and the AWRC. Suspended TiO_2 was added to lake samples, and lake water spiked with lab grown cyanobacteria and/or MC-LR solution to assess the efficacy of HAB treatment. For a 2-hour experiment, samples were taken every 30 minutes and analyzed for microcystin concentration through Eurofins Abraxis ELISA assays. All samples were analyzed in duplicate, and mean values were calculated. Student's t-test was used to compare between control and UV-treated samples.

Results and Discussion

Both suspended and attached TiO_2 experiments to treat cyanobacteria were repeated at least three times. Different from the MC-LR treatment, UV light did not enhance the TiO_2 treatment on cyanobacteria. Figure 1 shows the cyanobacteria flasks after the suspended and sprayed nets experiment. Figures 1A and 1B has visible flocs forming at the bottom of the flask, while the microscopy revealed no changes in cell morphology, indicating coagulation/flocculation by suspended NP was the main reaction mechanism. However, the sprayed nets did not change the cyanobacteria concentration significantly ($p = 0.87$) comparing to empty nets. No visible flocs were formed in the sprayed nets (Figure 1C), nor did the cell morphology change over time. The sprayed nets did catch some cyanobacteria, shown as the green color on the net after the experiment (Figure 1D). However, empty nylon nets also caught similar amount of cyanobacteria biomass, so we concluded the attached TiO_2 was not effective removing cyanobacteria from water.

Due to the ineffectiveness of sprayed nets on cyanobacteria treatment, only the suspended TiO_2 was applied in lake water experiment to assess the cyanotoxin removal in real water matrices. Nanoparticles were added to lake water and lake water spiked with cyanobacteria. Cyanotoxin level in lake water was already 12 ppb, so no additional MC-LR was spiked into lake water. Over 120 minutes, neither did cyanotoxin or cyanobacteria concentration change significantly, indicating the other constituents in lake water might have reacted with TiO_2 first, rendering the NP treatment on cyanotoxin ineffective.

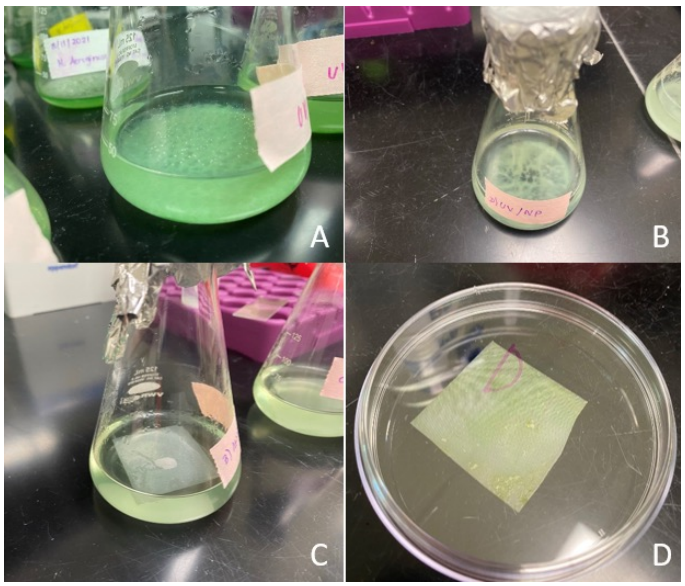

Figure 1: Cyanobacteria flasks after the TiO_2 NP treatment. 1A and B: cyanobacteria after suspended NP treatment; C: cyanobacteria after sprayed net experiment; D: sprayed net after the experiment.

Even though the results of the TiO_2 treatment of HAB was not desired, we did learn that NP treatment of MC-LR was highly effective when no other contaminants were present (DI water experiment in previous report). This implies TiO_2 treatment could be applied as a polishing step in drinking water treatment, especially considering minimal toxicity was reported for TiO_2. The NP treatment deserves further research to determine the best application format (suspended vs. packed column, etc.), and it could be a viable alternative treatment when HAB is of concern for certain water facilities, both in Arkansas and around the country.

Conclusions

TiO_2 nanoparticles was tested to treat cyanobacteria and cyanotoxins in HABs. Previous results showed the TiO_2 nanoparticles both in suspension and on sprayed nets were effective in degrading the most common cyanotoxin microcystin LR (MC-LR) in deionized water. However, when treating cyanobacteria, the suspended TiO_2 nanoparticles promote flocculation of cyanobacteria, while the TiO_2 net was unable to remove cyanobacteria biomass. Suspended TiO_2 nanoparticles was also applied to lake water, but they were unable to degrade MC-LR due to the presence of other constituents in lake water.

In conclusion the proposed TiO_2 net will not be a viable option for treating HAB in situ. However, TiO_2 nanoparticles could be applied as a polishing step to remove cyanotoxin from drinking water due to their effectiveness toward degrading MC-LR. This could be further explored by drinking water facilities when the water quality is challenged by HAB in the source water all over Arkansas and other states.

Acknowledgements

This material is based upon work supported by the United States Geological Survey under grant agreement No. G21AP10581 and administered by the Arkansas Water Resources Center. The views and conclusions contained in this document are those of the authors and should not be interpreted as representing the opinions or policies of the U.S. Geological Survey.

References

Anderson, D. M., P. M. Glibert and J. M. Burkholder (2002). "Harmful algal blooms and eutrophication: nutrient sources, composition, and consequences." Estuaries 25(4): 704-726.

Blaha, L., P. Babica and B. Marsalek (2009). "Toxins produced in cyanobacterial water blooms - toxicity and risks." Interdisciplinary Toxicology 2(2): 36-41.

Marsalek, B., D. Jancula, E. Marsalkova, M. Mashlan, K. Safarova, J. Tucek and R. Zboril (2012). "Multimodal action and selective toxicity of zerovalent iron nanoparticles against cyanobacteria." Environmental Science and Technology 46(4): 2316-2323.

Meglic, A., A. Pecman, T. Rozina, D. Lestan and B. Sedmak (2017). "Electrochemical inactivation of cyanobacteria and microcystin degradation using a boron-doped diamond anode - A potential tool for cyanobacterial bloom control." Journal of Environmental Science (China) 53: 248-261.

Meng, X., P. E. Savage and D. Deng (2015). "Trash to Treasure: From Harmful Algal Blooms to High-Performance Electrodes for Sodium-Ion Batteries." Environmental Science and Technology 49(20): 12543-12550.

Yang, Z., R. P. Buley, E. G. Fernandez-Figueroa, M. U. G. Barros, S. Rajendran and A. E. Wilson (2018). "Hydrogen peroxide treatment promotes chlorophytes over toxic cyanobacteria in a hyper-eutrophic aquaculture pond." Environmental Pollution 240: 590-598.

Zhou, Q., L. Li, L. Huang, L. Guo and L. Song (2018). "Combining hydrogen peroxide addition with sunlight regulation to control algal blooms." Environmental Science and Pollution Research 25(3): 2239-2247.

Zimba, P. V., L. Khoo, P. S. Gaunt, S. Brittain and W. W. Carmichael (2001). "Confirmation of catfish, Ictalurus punctatus (Fafinesque), mortality from Microcystis toxins." Journal of Fish Diseases 24: 41-47.

Arkansas Bulletin of Water Research

A publication of the Arkansas Water Resources Center

Brian E. Haggard
Director

Erin Grantz
Program Manager

Lillie Haddock
Program Specialist

University of Arkansas
Don Tyson Center for Agricultural Sciences
1371 W. Altheimer Drive
Room 106
Fayetteville, AR 72704

phone: 479-502-9854
email: egrantz@uark.edu

Visit our website: awrc.uada.edu

Call for Papers

Share your research results in a citable publication

To submit, go to awrc.uada.edu to view author instructions.

Partners

DIVISION OF AGRICULTURE
RESEARCH & EXTENSION
University of Arkansas System

The National Institutes for Water Resources

USGS
science for a changing world